Article

Current Biology

Disruption of Core Planar Cell Polarity Signaling Regulates Renal Tubule Morphogenesis but Is Not Cystogenic

Graphical Abstract

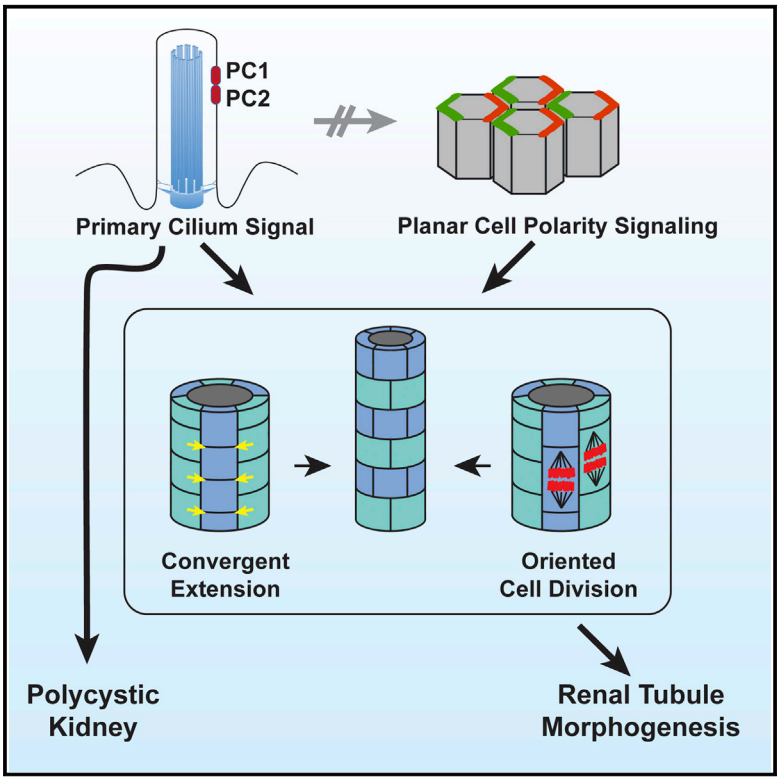

Highlights

- PCP signaling in kidney tubules controls uniformity of tubule diameter
- PKD mutations do not disrupt PCP signaling
- Primary cilia and PCP signaling provide independent control of CE and OCD
- Loss of PCP signaling does not induce cysts

Authors

Koshi Kunimoto, Roy D. Bayly, Eszter K. Vladar, Tyson Vonderfecht, Anna-Rachel Gallagher, Jeffrey D. Axelrod

Correspondence

jaxelrod@stanford.edu

In Brief

Although perturbation of oriented cell division is frequently associated with polycystic kidney disease, Kunimoto et al. show that blocking planar cell polarity (PCP) signaling is not cystogenic, nor is PCP disturbed in cysts induced by disruption of primary cilia. The commonly proposed model in which PCP regulates cystogenesis is thus incorrect.

Kunimoto et al., 2017, Current Biology 27, 3120–3131
October 23, 2017
https://doi.org/10.1016/j.cub.2017.09.011

CellPress

Current Biology
Article

Disruption of Core Planar Cell Polarity Signaling Regulates Renal Tubule Morphogenesis but Is Not Cystogenic

Koshi Kunimoto,[1] Roy D. Bayly,[1] Eszter K. Vladar,[1] Tyson Vonderfecht,[1] Anna-Rachel Gallagher,[2] and Jeffrey D. Axelrod[1,3,*]

[1]Department of Pathology, Stanford University School of Medicine, 300 Pasteur Drive, Stanford, CA 94305, USA
[2]Department of Internal Medicine, Yale School of Medicine, 333 Cedar Street, New Haven, CT 06520, USA
[3]Lead Contact
*Correspondence: jaxelrod@stanford.edu
https://doi.org/10.1016/j.cub.2017.09.011

SUMMARY

Oriented cell division (OCD) and convergent extension (CE) shape developing renal tubules, and their disruption has been associated with polycystic kidney disease (PKD) genes, the majority of which encode proteins that localize to primary cilia. Core planar cell polarity (PCP) signaling controls OCD and CE in other contexts, leading to the hypothesis that disruption of PCP signaling interferes with CE and/or OCD to produce PKD. Nonetheless, the contribution of PCP to tubulogenesis and cystogenesis is uncertain, and two major questions remain unanswered. Specifically, the inference that mutation of PKD genes interferes with PCP signaling is untested, and the importance of PCP signaling for cystogenic PKD phenotypes has not been examined. We show that, during proliferative stages, PCP signaling polarizes renal tubules to control OCD. However, we find that, contrary to the prevailing model, PKD mutations do not disrupt PCP signaling but instead act independently and in parallel with PCP signaling to affect OCD. Indeed, PCP signaling that is normally downregulated once development is completed is retained in cystic adult kidneys. Disrupting PCP signaling results in inaccurate control of tubule diameter, a tightly regulated parameter with important physiological ramifications. However, we show that disruption of PCP signaling is not cystogenic. Our results suggest that regulating tubule diameter is a key function of PCP signaling but that loss of this control does not induce cysts.

INTRODUCTION

Polycystic kidney disease (PKD) is a prominent feature of single-gene heritable genetic disorders, including autosomal dominant PKD, autosomal recessive PKD, and others (reviewed in [1, 2]). A striking commonality of single-gene PKDs is that the affected proteins function in or contribute to the structure or function of primary cilia [3, 4]. The importance of primary cilia in the etiology of PKD is well documented. However, the developmental and disease-inducing processes affected by primary cilia in the kidney are not well understood.

Two morphogenetic processes, convergent extension (CE) and oriented cell division (OCD), have been proposed to regulate kidney tubule morphogenesis, and their disruption has been associated with development of PKD. CE describes the reorganization of cells to elongate one tissue axis and narrow the orthogonal axis such that, in the renal tubule, CE would reduce tubule diameter [5, 6]. CE has been directly observed by live imaging in the *Xenopus* nephron [7]. In fixed tissues, CE may be inferred by cellular elongation in the direction of migration and, by this method, has been implicated in mouse nephron morphogenesis [8, 9]. Defective inferred CE precedes cystogenesis in *Wnt9b* [8] and *Pkd1* [9] mouse mutant collecting ducts, but the appealing hypothesis that impaired CE leads to cyst formation has not been directly examined.

OCD, if aligned with the tubule axis, is expected to maintain tubule diameter while facilitating elongation during proliferative growth and has been documented during embryonic and postnatal tubule elongation [8, 10–17]. Perturbation of OCD has been associated with development of PKD [8, 10–12, 14, 15], though whether loss of OCD occurs before or after cystogenesis is controversial [14, 15]. Nonetheless, perturbation of OCD is neither necessary nor sufficient to cause cysts, as impaired OCD is observed in *Wnt7b* and *Pkhd1* (causative of autosomal recessive polycystic kidney disease [ARPKD] in humans) mutant mouse kidneys, yet they do not develop cysts [13, 15], and mutation of *Ift140*, a cilium component, causes cysts without perturbing OCD [16]. Thus, CE and OCD are both integral to normal renal tubule development, but their relationship to PKD is less clear.

PCP signaling controls the polarity of numerous epithelia in both *Drosophila* and vertebrates and regulates both OCD and CE in various contexts [18]. The *Drosophila* wing, in which each cell produces a trichome that emerges from the distal side of the cell, has been an instructive model of PCP signaling, revealing a modular signaling system composed of genetically and biochemically related units [19]. The "core" module acts both to amplify asymmetry and to coordinate polarization between neighboring cells, producing a local alignment of polarity. Proteins in the core module, including the transmembrane

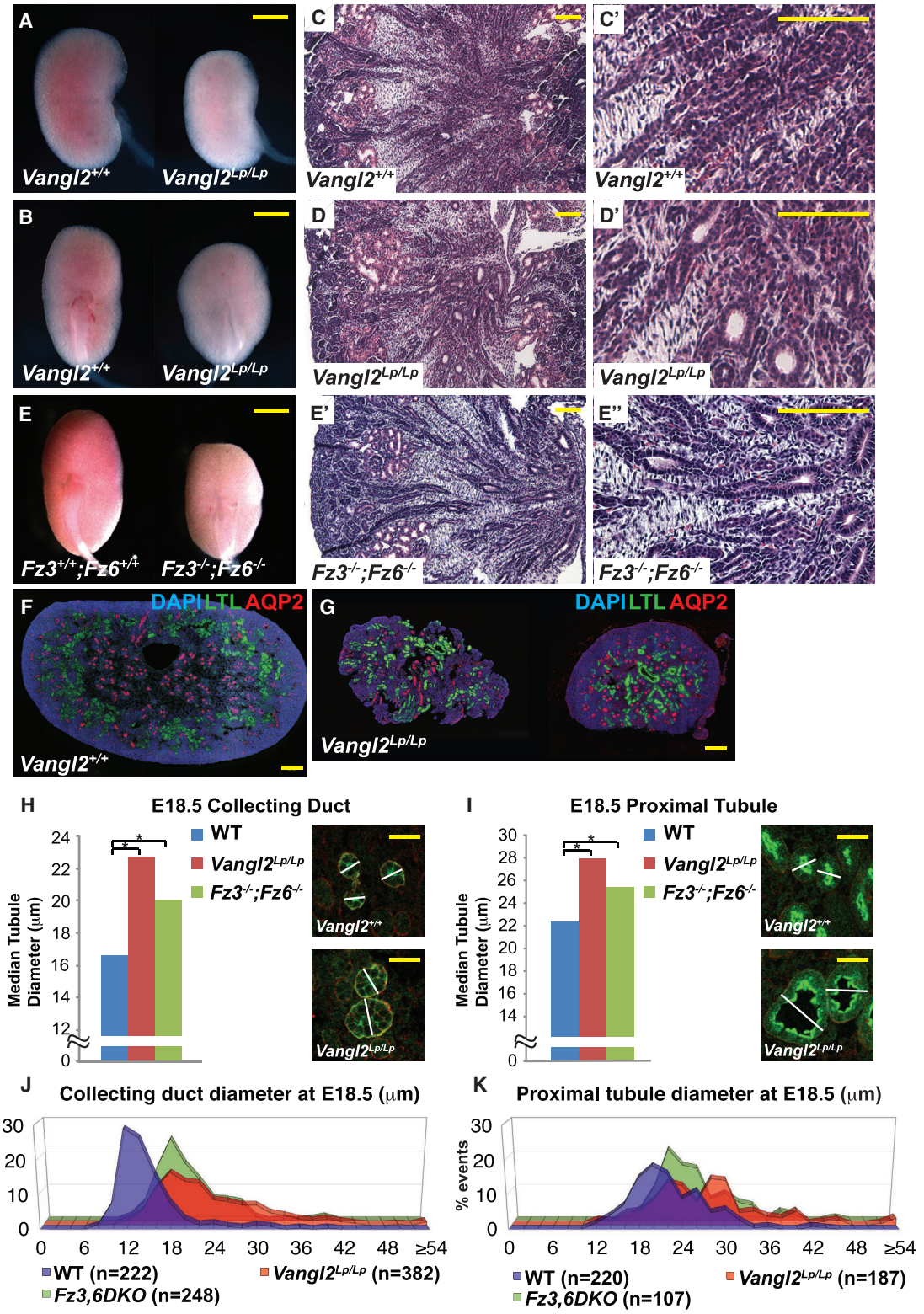

Figure 1. Phenotypes of WT, *Vangl2*$^{Lp/Lp}$, and *Fz3*$^{-/-}$; *Fz6*$^{-/-}$ Mutant Kidneys at E18.5

(A and B) Lateral (A) and hilar (B) views of control and *Vangl2*$^{Lp/Lp}$ kidneys.

(C–D') Low (C and D) and high (C' and D') power H&E histology of control and *Vangl2*$^{Lp/Lp}$ kidneys.

(E) *Fz3*$^{-/-}$; *Fz6*$^{-/-}$ kidneys.

(E' and E") Low (E) and high power (E') H&E histology of *Fz3*$^{-/-}$; *Fz6*$^{-/-}$ kidneys.

(legend continued on next page)

proteins Frizzled (Fz), Flamingo/Starry night (Fmi), Van Gogh/Strabismus (Vang), and the cytosolic/peripheral membrane proteins Dishevelled, Diego, and Prickle, adopt asymmetric subcellular localizations that predict morphological polarity patterns, such as trichome orientation. These proteins communicate at cell boundaries, recruiting one group to the distal side of cells and the other to the adjacent proximal side through the function of a feedback mechanism, thereby aligning the polarity of adjacent cells [20, 21] (reviewed in [18, 22]).

Downstream of the core module, tissue-specific "effector" modules orchestrate morphological responses to the molecular asymmetry produced by core module function. Upstream of the core module, several "global" modules have been proposed to link the direction of core module polarization to tissue axes. One of these, comprising the atypical cadherins Fat (Ft), Dachsous (Ds), and the Golgi protein Four-jointed, converts opposing tissue-level expression gradients of Four-jointed and Ds into subcellular asymmetry of intercellular Ft-Ds heterodimers that align PCP with the tissue axes [23]. In addition, Wnts and other unknown signals have been implicated as global regulators [24, 25].

In many vertebrate tissues, characteristic features of the PCP signaling mechanism identified in flies are conserved. Yet, in various contexts, features of the mechanism have been adapted and evolved [6, 26], and some PCP genes function in mechanisms other than PCP [18]. Furthermore, whereas *Drosophila* has one, or in a few cases, two paralogs of essential PCP genes, vertebrates typically have three or more paralogs, suggesting redundancy and/or diversification of function.

The contribution of PCP-related events, and hence core PCP signaling, to PKD was first proposed based on the observation that OCD is observed along the length of the tubule axis and is disturbed prior to cystogenesis in a model of PKD [10]. The inference or observation of CE in renal tubule morphogenesis reinforced this idea [7, 8]. However, evidence implicating the PCP signaling mechanism per se in kidney morphogenesis or in PKD is circumstantial. Numerous Wnts are associated with loss of OCD and/or cysts, but assigning function to PCP versus other pathways is challenging [8, 13, 27, 28]. Mutations in Inversin, a homolog of *Drosophila* Diego, cause nephronophthisis type 2 [29]; however, the association of Inversin with cilia and with both canonical Wnt as well as PCP signaling makes interpretation difficult (reviewed in [30]). Loss of FAT4, the closest vertebrate ortholog of *Drosophila* Ft [31], results in disruption of OCD and in very dilated, possibly cystic embryonic tubules [11]. Furthermore, FAT4 and DCHS1 may form a heterodimer pair analogous to *Drosophila* Ft-Ds [11, 32, 33]. The *Fat4* dilated tubule/cystic phenotype was enhanced by *Vangl2* heterozygosity, possibly connecting global and core PCP signaling to OCD and cystogenesis. In contrast, *Vangl2*$^{Lp/Lp}$ mutant animals show tubule branching and glomerular defects, but not cysts, at embryonic day 18.5 (E18.5) [34]. Confounding a simple interpretation, FAT4 is mostly expressed in the stroma, whereas DCHS1 is primarily expressed in the metanephric mesenchyme [33].

Studies of additional PCP signaling components have suggested a role for PCP in kidney morphogenesis. Xdd1, a dominant-negative DISHEVELLED derivative, disrupts CE in the frog kidney [7]. However, the association of DISHEVELLED with basal bodies suggests that basal body docking or other ciliary defects may account for this phenotype [35]. Similarly, knockdown of *pk1* in the Zebrafish kidney disorganizes basal bodies and produces cysts. However, genetic interaction with intraflagellar transport (IFT) mutants and the known functions of Pks in regulating the cytoskeleton are also consistent with non-PCP mechanisms [24, 36, 37]. Misoriented OCD is observed in *Celsr1*$^{-/-}$ (ortholog of *Fmi*) and *Celsr1*$^{+/-}$;*Vangl2*$^{Lp/+}$ mutant kidneys [17], providing additional evidence for a role of PCP signaling in tubule morphogenesis. Yet, the characteristic subcellular localization of core PCP components that would substantiate conserved PCP signaling function remains to be demonstrated.

Planar polarized behaviors occur in renal tubule morphogenesis, and evidence cited above suggests that they are controlled by PCP signaling. However, two major questions remain unanswered. Specifically, the inference that mutation of PKD genes interferes with PCP signaling is untested, and the importance of PCP signaling for cystogenic PKD phenotypes has not been examined. We therefore directly and functionally interrogated PCP signaling in the mouse kidney.

RESULTS

Core PCP Components Are Required for Proper Kidney and Tubule Morphology

To determine whether the core PCP pathway is required for kidney tubule morphogenesis, we analyzed kidney development in mice mutant for *Vangl1*, *Vangl2*, *Fz3*, and *Fz6* separately and in combination. *Vangl2*$^{Lp/Lp}$ homozygotes die at birth. At E18.5, their kidneys were shorter and wider than wild-type littermates, as previously reported [34], and their tubules appeared mildly dilated (Figures 1A–1D'). In contrast, *Vangl1*$^{-/-}$ mice (likely hypomorphs) are viable, fertile, with kidneys macroscopically similar to those of wild-type littermates (data not shown). Similar to *Vangl1*$^{-/-}$, the kidneys of *Fz3*$^{-/-}$ and *Fz6*$^{-/-}$ single-mutant mice were not obviously affected (data not shown). *Fz3*$^{-/-}$;*Fz6*$^{-/-}$ double-mutant mice die perinatally with multiple PCP-related phenotypes [38]. Their kidneys were shorter and wider than wild-type littermates and showed dilated tubules comparable to those in *Vangl2*$^{Lp/Lp}$ kidneys (Figures 1E–1E").

In both *Vangl2*$^{Lp/Lp}$ and *Fz3*$^{-/-}$;*Fz6*$^{-/-}$ kidneys at E18.5, median tubule diameters of both collecting ducts and proximal tubules were significantly larger compared to wild-type

(F and G) Immunofluorescence images of control (F) and *Vangl2*$^{Lp/Lp}$ (G) kidneys stained for DAPI (blue; nuclei), LTL (green; proximal tubule), and AQP2 (red; collecting duct).

(H and I) Median tubule diameters for wild-type (WT) control, *Vangl2*$^{Lp/Lp}$, and *Fz3*$^{-/-}$; *Fz6*$^{-/-}$ collecting ducts (H) and proximal tubules (I). Images illustrate measurement method (see STAR Methods). Asterisks indicate significant differences: (H) 22.7 μm and 20.1 μm, respectively, versus 16.6 μm for WT control; *$p < 0.0001$ and (I) 28.0 μm and 25.4 μm, respectively, versus 22.4 μm for WT control; *$p < 0.0001$ by Mann-Whitney U test.

(J and K) Distribution plots of data from (H) and (I) (J and K, respectively).

The scale bars represent (A, B, and E) 1 mm, (C–E") 100 μm, (F and G) 200 μm, and (H and I) 25 μm. See also Figure S1.

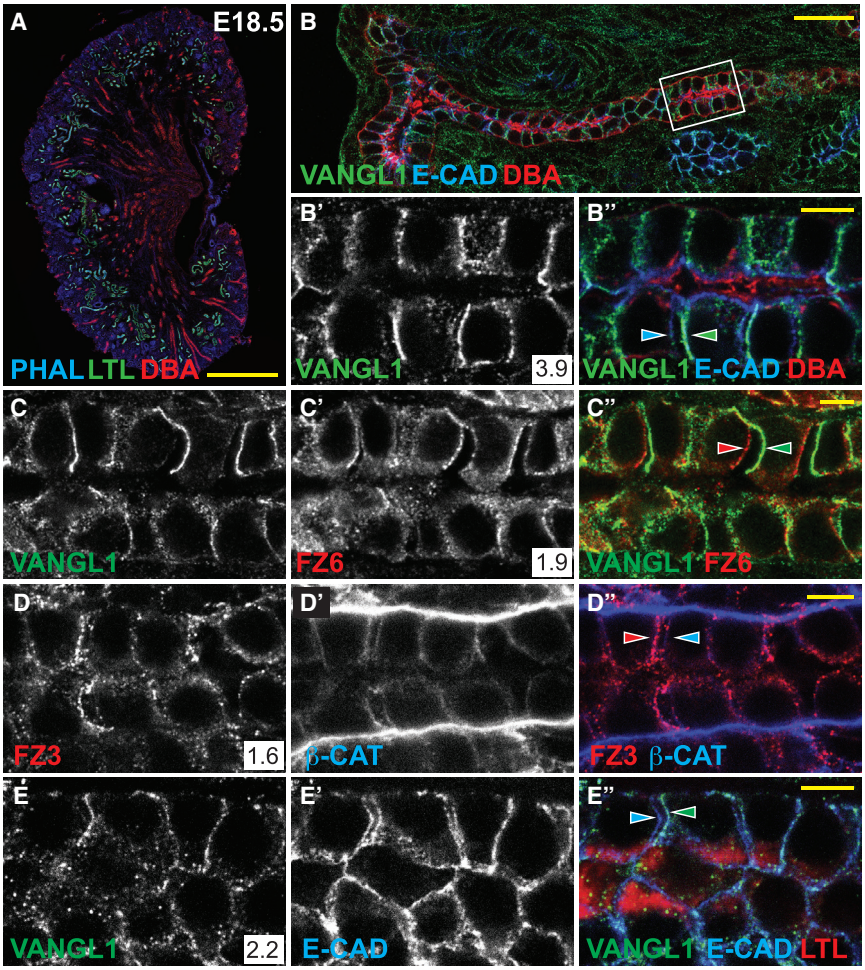

Figure 2. Core PCP Proteins Localize Asymmetrically in Proximal Tubule and Collecting Duct

(A) Control kidney stained for PHALLOIDIN (blue; actin), LTL (green; proximal tubule), and DBA (red; collecting duct).

(B–B'') Collecting duct stained for VANGL1 (green) and E-CAD (blue), showing asymmetric proximal localization of VANGL1 relative to E-CAD (arrowheads).

(C–C'') Collecting duct stained for VANGL1 (green) and FZ6 (red), showing asymmetric proximal localization of Vangl1 and distal localization of FZ6 (arrowheads).

(D–D'') Collecting duct showing distal localization of FZ3 (red) relative to β-CATENIN (blue).

(E–E'') Proximal tubule (LTL; red) showing proximal localization of VANGL1 (green) relative to E-CAD (blue; arrowheads).

Asymmetry was quantified as an intensity ratio (see STAR Methods) and indicated in the white box in associated figure panels and graphically in Figure S3C. The scale bars represent (A) 500 μm, (B) 25 μm, and (B'', C'', D'', and E'') 5 μm. See also Figure S2.

littermates (Figures 1F–1I). Enlarged diameters were also observed for *Vangl1*$^{-/-}$ mutant tubules (Figure S1; related to Figure 1). Importantly, plots of these measurements revealed a substantially broader distribution in the mutants compared to wild-type (Figures 1J, 1K, and S1; related to Figure 1). Core PCP components therefore shape the kidney by regulating the diameter of renal tubules. The mutants examined here have not been implicated in ciliogenesis, and we detected no alteration in cilia morphology.

Core PCP Components Are Asymmetrically Localized along the Proximal-Distal Tubule Axis

We investigated whether core components of the PCP pathway function in tubule epithelia and whether they function in a conserved PCP signaling mechanism. At E18.5, when each stage of nephrogenesis is present (Figure 2A), VANGL1, VANGL2, FZ3, and FZ6 were detected in all tubule segments, primarily in the lateral membranes of epithelial cells with a diffuse cytosolic presence (Figures 2B, 2B', and 2D–2E''; data not shown). This pattern was observed as early as E13.5 and persisted into early postnatal development, after which membrane localization dissipated over several weeks (Figures S2A–S2I; related to Figure 2; Figures 7C–7C'''). Consistent with this decline, mRNA expression of multiple core PCP genes and related factors decreased between postnatal day 1 (P1) and 16 weeks (Figure S2J; related to Figure 2). These observations suggest that developing tubule cells participate in PCP signaling but that tubules in a post-proliferative quiescent state no longer engage in PCP signaling.

Using a low-calcium dehydration step prior to fixation that induced separation of a fraction of cell-cell junctions, we reliably observed the selective asymmetric accumulation of VANGL1 and VANGL2 along the proximal side and FZ3 and FZ6 along the distal side of cells in both the collecting duct and proximal tubules (Figures 2B–2E''). This asymmetric localization is indicative of active PCP signaling and is strongly reminiscent of that first observed in *Drosophila* and subsequently in numerous vertebrate tissues.

A characteristic feature of PCP signaling is the dependence of each core protein's asymmetric localization on the activity of the other core proteins. In *Vangl2*$^{Lp/Lp}$ mice, in which strong kidney tubule phenotypes are observed (Figure 1), asymmetry of VANGL1, FZ3, and FZ6 localization was eliminated. In addition, their distributions were more punctate, and levels of VANGL1 in particular were decreased (likely due to the dominant-negative activity of the Lp allele; Figures 3A–3C'') [39]. Similarly, in *Fz3*$^{-/-}$;*Fz6*$^{-/-}$ mice, whose phenotype is comparable to that of *Vangl2*$^{Lp/Lp}$ mice, asymmetry of VANGL1 and VANGL2 localization was significantly diminished, though not eliminated (Figures 3D–3D'' and S3B–S3B''; related to Figure 3; data not shown). This contrasts with *Fz3*$^{-/-}$;*Fz6*$^{+/-}$ and *Fz3*$^{+/-}$;*Fz6*$^{-/-}$ mice, in which the asymmetry of VANGL1 and VANGL2 was not diminished (Figures S3A–S3A''; related to Figure 3; data not shown). In *Vangl1*$^{-/-}$ tubules, the asymmetric localization of VANGL2, FZ6, and FZ3 was modestly diminished, perhaps

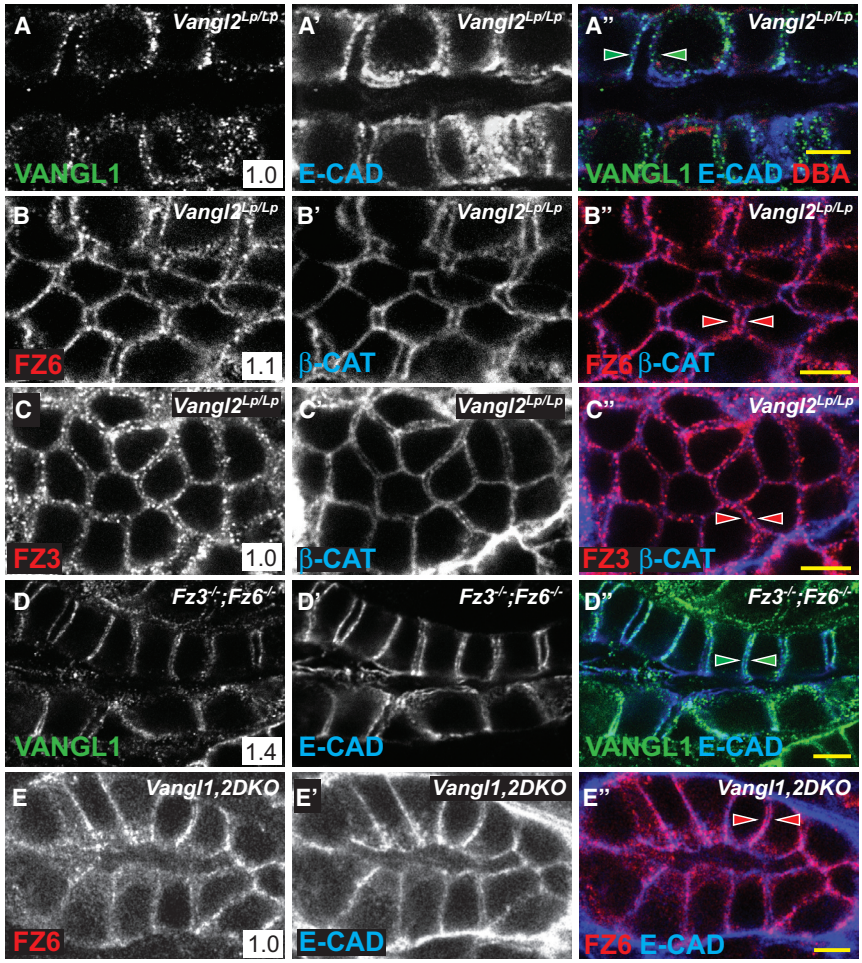

Figure 3. Asymmetric Localization of Core PCP Protein Localization Is Lost in PCP Mutants

(A–C) E18.5 *Vangl2*$^{Lp/Lp}$ collecting ducts (DBA, red) stained for (A) VANGL1 (green) and E-CAD (blue), (B) FZ6 (red) and E-CAD (blue), or (C) FZ3 (red) and E-CAD (blue), showing similar proximal and distal localization of VANGL1, FZ6, and FZ3 (arrowheads).

(D) E18.5 *Fz3*$^{-/-}$; *Fz6*$^{-/-}$ collecting duct stained for VANGL1 (green) and E-CAD (arrowheads).

(E) P1 *Vangl1*,*2DKO*, *Ksp-Cre* collecting duct stained for FZ6 (red) and E-CAD (blue).

The scale bars represent 5 μm. See also Figure S3.

due to the hypomorphic nature of the allele or to redundancy between *Vangl1* and *Vangl2* (Figures S3B–S3B''; related to Figure 3; data not shown). The core components are therefore mutually required for establishment and/or maintenance of their asymmetric localization, indicating that they function in a conserved PCP signaling mechanism to regulate tubule diameter.

Effects of PCP Mutation on Postnatal Tubules

The mutants examined thus far are perinatally lethal, precluding analyses of potential adult kidney phenotypes. Furthermore, observations from systemic mutants do not rule out the possibility of non-autonomous perturbation of tubule development. We therefore made conditional *Vangl1*/*Vangl2* double knockouts targeted to the collecting ducts from early branching ureteric bud stage (*Vangl1*,*2DKO*, *Ksp-Cre*; see STAR Methods). Eliminating the only two Vangl paralogs is expected to severely compromise or abolish core PCP signaling. *Vangl1*,*2DKO*, *Ksp-Cre* animals were viable and survived long into adulthood, and recombination in collecting ducts was complete (Figures S4A–S4B''). Asymmetry of FZ6 localization was abolished, confirming effectively complete disruption of core PCP signaling (Figures 3E–3E''). Macroscopically, *Vangl1*,*2DKO*, *Ksp-Cre* kidneys showed no apparent phenotype (Figures S4C and S4D). However, collecting ducts observed in thick sections showed irregular morphology compared to wild-type, consistent with varying duct diameter (Figures 4A and 4B). We therefore measured collecting duct diameter of P1 *Vangl1*,*2DKO*, *Ksp-Cre* animals. Because, to this point, diameter measurements were performed in samples prepared in low-calcium dehydration conditions, we first verified that standard fixation (see STAR Methods) produced comparable results by repeating measurements on E18.5 *Vangl2*$^{Lp/Lp}$ kidneys. These samples showed an identical trend but with larger absolute values due to lack of dehydration (Figures S4E–S4H; related to Figure 4). With standard fixation, P1 *Vangl1*,*2DKO*, *Ksp-Cre* collecting ducts showed broader diameter distribution compared to wild-type (Figure 4E), much like the E18.5 *Vangl2*$^{Lp/Lp}$ and *Fz3*$^{-/-}$;*Fz6*$^{-/-}$ mutants, and median diameter was larger than wild-type but less dramatically so. PCP therefore impacts tubule diameter into the postnatal period and is required autonomously in ductal epithelial cells.

Loss of Tubule PCP Is Not Cystogenic

Because disruption of PCP has been proposed to be cystogenic, we aged the *Vangl1*,*2DKO*, *Ksp-Cre* mice for up to 50 weeks. Remarkably, and contrary to common conjecture, none of 17 animals aged from 3 to 50 weeks (Table S1) developed renal cysts (Figures 4C–4D'''). Indeed, median tubule diameter continued to decrease into adulthood as it did in wild-type. The median diameter of *Vangl1*,*2DKO*, *Ksp-Cre* collecting ducts at 16 weeks decreased compared to P1 yet remained somewhat larger than wild-type, and diameter distribution was broader (Figure 4F). PCP is therefore required to ensure the uniformity of tubule diameters throughout development. During embryogenesis, mutant tubules decrease their diameter less uniformly and reliably than wild-type tubules, leading to both a larger median diameter and a broader diameter distribution. Postnatally, wild-type and mutant tubules continue to decrease in diameter, presumably by a PCP independent process, but the non-uniformity of PCP mutant tubule diameters remains.

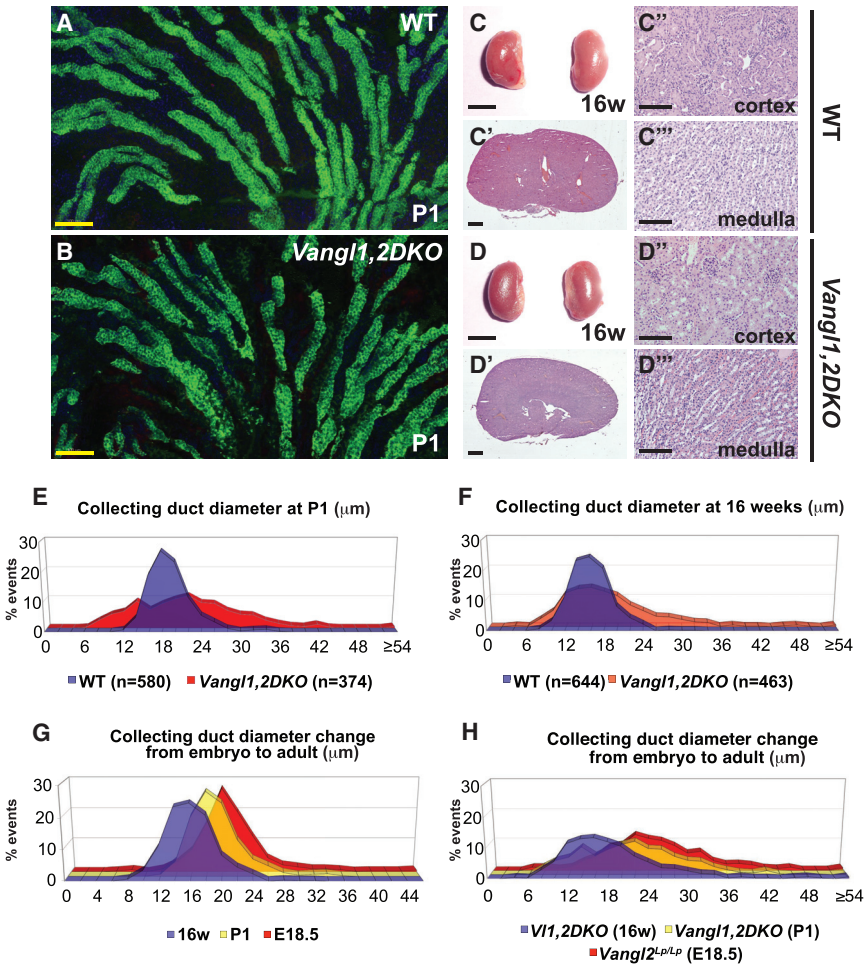

Figure 4. Phenotype of *Vangl1,2DKO* Kidneys at P1 and 16 Weeks

(A and B) Longitudinal sections of WT control (A) and *Vangl1,2DKO* (B) collecting ducts stained for AQP2 (marking lumens) showing more irregular diameter of the *Vangl1,2DKO* ducts along their lengths. Samples are 30 μm thickness. See also Movies S1 and S2.

(C–D''') Gross and H&E sections of WT control (C–C''') and *Vangl1,2DKO* (D–D''') mutant kidneys showing absence of cysts.

(E and F) Distribution plots of collecting duct diameters of WT and *Vangl1,2DKO* at P1 (E) and 16 weeks (F), measured with standard fixation, showing broader distribution in *Vangl1,2DKO* compared to WT.

(G and H) Distribution plots of collecting duct diameters showing reduction in overall diameters from E18.5 to 16 weeks in both WT (G) and mutant (H) ducts.

The scale bars represent (A, B, C'', C''', D'', and D''') 100 μm, (C and D) 5 mm, and (C' and D') 1 mm. See also Figure S4 and Table S1.

PCP Signaling Controls Cellular Rearrangement and Oriented Cell Divisions

PCP-dependent CE, whereas only inferred in mice, is hypothesized to underlie narrowing of tubule diameter and concurrent reduction in the number of cells comprising tubule circumference [8, 9]. We therefore measured cell number in circumferential cross-sections of tubules over time. As previously described [8, 9], the cross-sectional cell number in wild-type collecting ducts and proximal tubules decreases throughout embryonic development, with the most marked reduction occurring between E16.5 and E18.5 (Figure 5A). However, in *Vangl2*$^{Lp/Lp}$ mutants, collecting duct cross-sectional cell number decreases more slowly, with the most dramatic difference between mutant and wild-type observed at E17.5, suggesting a maximum perturbation of processes occurring between E16.5 and E17.5. The difference between wild-type and mutant persisted through E18.5. A similar effect was observed in proximal tubules (Figure 5B). In both tubule types, the decline in cell counts in mutants was slowed, but not arrested. Thus, either *Vangl2*$^{Lp/Lp}$ only partially disrupts the relevant mechanism(s) or fully inhibits only a subset of several mechanisms that lead to the reduction in cross-sectional cell number. Due to the difficulty in breeding *Fz3*$^{-/-}$;*Fz6*$^{-/-}$ mice, we were only able to analyze tubules at E18.5. Their cross-sectional cell number was very similar to that of *Vangl2*$^{Lp/Lp}$ mice (Figures 5A and 5B).

Convergent extension is reflected in cellular elongation in the direction of cell intercalation [6]. Unlike previous reports, we observe a bimodal distribution of orientations in wild-type tubules during narrowing, but like *Wnt9b*$^{-/-}$ mutants that fail to efficiently narrow collecting duct diameters [8], cellular long axes in *Vangl2*$^{Lp/Lp}$ tubules were shifted toward the tubule axis compared to wild-type (Figure S5; related to Figure 5). These results support existing evidence that core PCP factors control cellular orientation and CE during the embryonic phase of renal tubule diameter reduction.

PCP Signaling Controls Oriented Cell Division in Tubules

Whereas oriented cell divisions are largely parallel to the tubule axis in wild-type tubules [10], off-axis cell division has been observed in a variety of mutants associated with polycystic kidney disease [10, 11, 13, 15, 16] and is also observed in *Pkhd1*$^{del4/del4}$ mouse mutants, which do not develop cysts [15]. We found that, in P1 *Vangl1,2DKO*, *Ksp-Cre* collecting ducts, cell division orientations are significantly off axis relative to the largely parallel wild-type divisions (Figures 5C and 5D; Movies S1 and S2). Therefore, PCP signaling regulates renal tubular OCD.

Primary Cilia Regulate Planar Polarized Behaviors, but Not Core PCP Signaling

Many cilium-associated PKD genes, as well as early genetic ablation of primary cilia (through loss of Kif3a) that result in the development of cysts by P30 [40], also show defective CE and OCD. This observation led to the hypothesis that these mutations induce cystogenesis, at least in part, by disrupting PCP signaling. Indeed, results from multiple systems have led to

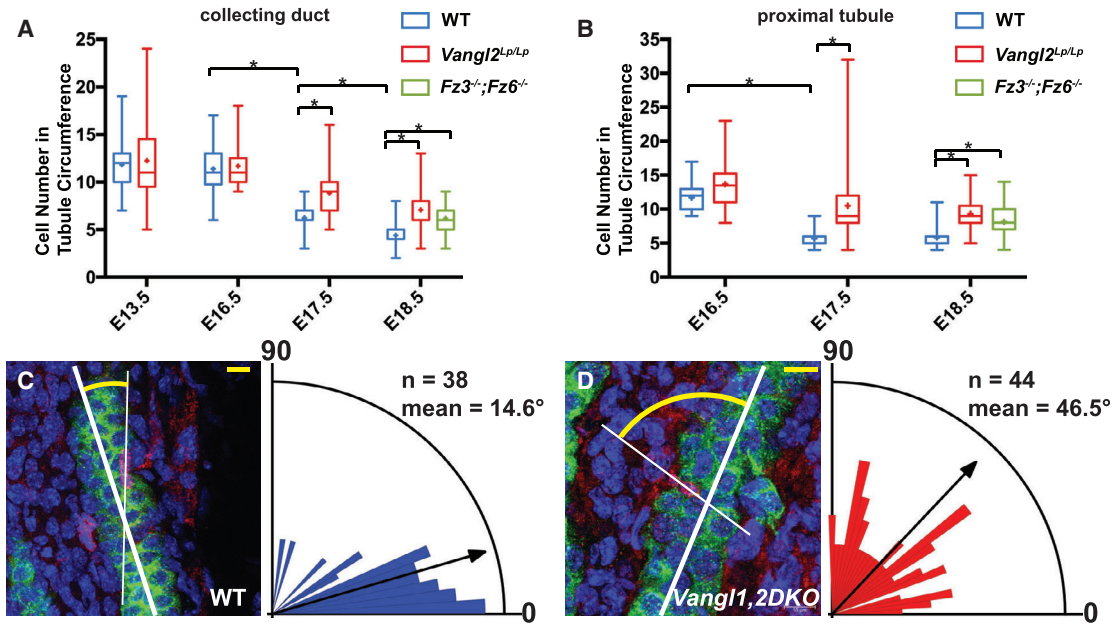

Figure 5. CE and OCD in WT and *Vangl1,2DKO* Collecting Ducts

(A and B) Cell number per tubule cross-section at the indicated stages in WT control, *Vangl2*$^{Lp/Lp}$, and *Fz3*$^{-/-}$;*Fz6*$^{-/-}$ collecting ducts (A) and proximal tubules (B), showing a slowed decrease in mutants compared to WT. Box and whisker format shows the minimum, lower quartile, median, upper quartile, and maximum values; + indicates mean. *$p < 0.0001$ by Mann-Whitney U test.

(C and D) Orientation of cell divisions in WT control (C) and in *Vangl1,2DKO* (D) collecting ducts assayed using the HISTONE H3 immunolabeling method [10], quantified at P1. Difference between WT control and Vl1,2DKO is significant at $p < 0.0001$ by Mann-Whitney U test. Representative images show cell divisions labeled for AQP2 (green; collecting duct), histone H3 (red; dividing nuclei), and DAPI (blue; all nuclei).

See also Movies S1 and S2 and Figure S5. The scale bars represent 10 μm.

proposals of a mechanistic relationship between PCP signaling and primary cilia, yet no clear understanding of the hypothesized relationship has emerged [41]. We therefore examined the relationship between primary cilia and PCP in renal tubule development.

We determined whether primary cilia contribute to regulation of tubule diameter during embryonic tubulogenesis, a time when PCP signaling contributes to this process. In *KspCre*;*Kif3a*$^{cko/cko}$ mice at E18.5, cilia were nearly ablated from collecting duct cells, leaving only short ciliary remnants (Figures S6B and S6C; related to Figure 6). In these kidneys, the median diameter of collecting duct tubules was significantly increased and the distribution broadened compared to wild-type, comparable to *Vangl2*$^{Lp/Lp}$ and *Fz3*$^{-/-}$;*Fz6*$^{-/-}$ kidneys (Figures 6A and 6B). Kif3a deletion also had an effect similar to that of the PCP mutants on both the cross-sectional cell number as well as on the distribution of cellular orientations with respect to the tubule axis (Figures 6C and S6A; related to Figure 6). These similar phenotypes may be explained either by dependence of PCP on primary cilia or vice versa or by their independent activity on CE and OCD.

We therefore examined PCP signaling in *KspCre*;*Kif3a*$^{cko/cko}$ mutants by assaying asymmetric PCP factor localization. At E18.5, VANGL1 and FZ6 retain their oppositely oriented asymmetric localization, indicating that core PCP signaling is intact (Figure 6D; data not shown). Thus, a reduction of primary cilia length sufficient to cause a tubule diameter defect similar to that seen in the core PCP mutant kidneys showed no effect on core PCP signaling. Primary cilia therefore appear to influence tubule diameter independent of core PCP signaling. However, because ciliary remnants still exist in *KspCre*;*Kif3a*$^{cko/cko}$ mice at E18.5, these data do not strictly rule out the possibility that renal tubule cilia may be required for generation or maintenance of core PCP factor asymmetric localization.

Pkhd1$^{del4/del4}$ mutant mice, which do not develop cysts, show off-axis cell division [15], and median tubule diameter is increased and more broadly distributed than wild-type, albeit modestly (Figure S6D; related to Figure 6). As in *Kif3a*$^{cko/cko}$, core PCP proteins VANGL1 and FZ6 retain their asymmetric localization in P1 *Pkhd1*$^{del4/del4}$ mutant collecting ducts (Figures 6E–6E''), indicating that the off-axis cell division in these mutants cannot be attributed to disruption of PCP signaling. Together, these results suggest that PCP signaling is intact when tubule cilia are mutated and are reminiscent of the findings that Ift88 mutation in the cochlea disrupts sensory hair cell polarity and that Kif3a knockout in ependymal cells disrupts basal body polarity, each without altering PCP protein asymmetry [42, 43].

Robust Asymmetric Localization of Core PCP Components Persists in Cyst-Lining Cells

Several weeks into adulthood, PCP signaling in wild-type ducts is substantially diminished. We therefore determined whether PCP signaling is similarly diminished in P30 Kif3a$^{cko/cko}$ mutant collecting ducts when Kif3a protein is depleted, cilia are severely shortened, and a strongly cystic phenotype is observed as

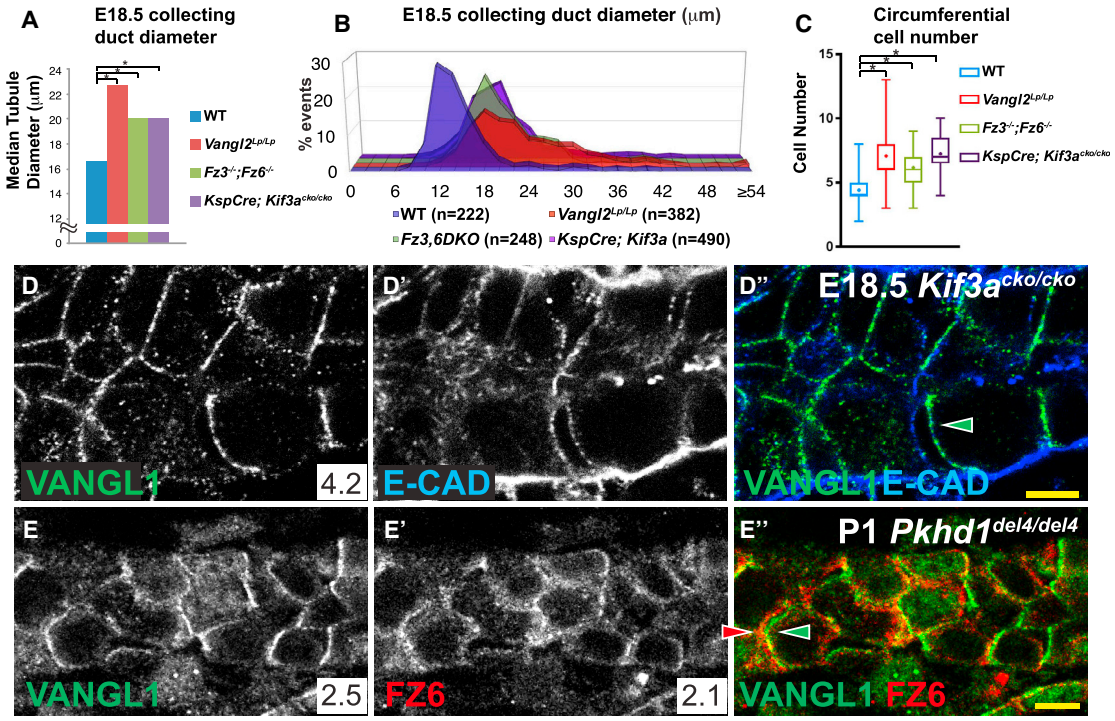

Figure 6. PCP in Cystic Kidneys

(A) Median collecting duct diameters at E18.5 for WT control, *Vangl2*$^{Lp/Lp}$, *Fz3*$^{-/-}$; *Fz6*$^{-/-}$, and *KspCre*;*Kif3a*$^{cko/cko}$. Data for WT control, *Vangl2*$^{Lp/Lp}$, and *Fz3*$^{-/-}$; *Fz6*$^{-/-}$ are from Figure 1H. For *KspCre*;*Kif3a*$^{cko/cko}$, median = 20.1 μM and *p < 0.0001 compared to wild-type by Mann-Whitney U test.

(B) Distribution plots of the measurements from (A).

(C) Circumferential cell number for E18.5 collecting ducts for WT control, *Vangl2*$^{Lp/Lp}$, *Fz3*$^{-/-}$; *Fz6*$^{-/-}$, and *KspCre*;*Kif3a*$^{cko/cko}$. Data are displayed in box and whisker format, showing the minimum, lower quartile, median, upper quartile, and maximum values; + indicates mean. *p < 0.0001 by Mann-Whitney U test. Data for WT control, *Vangl2*$^{Lp/Lp}$, and *Fz3*$^{-/-}$; *Fz6*$^{-/-}$ are from Figure 5A.

(D–D'') E18.5 collecting duct from *KspCre*;*Kif3a*$^{cko/cko}$ precystic kidneys showing asymmetrically localized VANGL1 (green); E-CAD (blue).

(E–E'') P1 *Pkhd1*$^{del4/del4}$ collecting duct showing asymmetrically localized VANGL1 (green) and FZ6 (red).

The scale bars represent 5 μm. See also Figure S6.

previously reported [40] (Figures 7A–7B'). Whereas in unaffected P30 proximal tubules, levels of VANGL1 and FZ6 at the lateral cell membrane were significantly diminished from P1 levels (Figures 7C–7C'''), in the cyst-lining cells of *KspCre*;*Kif3a*$^{cko/cko}$ mice, cilia were absent, and strikingly, localization of core PCP components was similar to that observed prenatally. Robust VANGL1 and FZ6 expression co-localized with E-CADHERIN (E-CAD) along the lateral membrane of tubule cells (Figures 7D–7D''', compare to Figures 7C–7C'''; Figures S6F–S6F'', compare to Figures S6E–S6E''; related to Figure 7) and was asymmetric in cyst-lining cells, identical to that observed embryonically (Figures 7E–7E'' and S6G–S6G''; related to Figure 6; Movie S1). Consistent with these observations, FZ3 was previously found to be elevated in cysts, though asymmetric localization was not noted [14]. We were unable to determine the global orientation (proximal-distal axis) of cysts and thus cannot rule out a potential disruption to orientation of polarity with respect to the tubule axis. These results demonstrate that, in renal tubule cells, PCP signaling, as revealed by the asymmetric subcellular localization of core PCP proteins, does not depend on primary cilia. Indeed, in adult (P30) kidneys, at a developmental stage at which PCP signaling is no longer active in wild-type, cystic tubule epithelia maintain or restore PCP signaling, perhaps because tubules are inappropriately in an embryonic-like, proliferative state.

DISCUSSION

It has been hypothesized that disruption of PCP, and therefore disruption of CE and OCD, contributes to PKD in a variety of cilium-associated mutant conditions. However, we find that, contrary to prior conjecture, not only is disruption of PCP signaling not required for cystogenesis but PCP signaling is retained in adult cysts when it would otherwise be attenuated. We suggest that PCP signaling is part of the developmental program in proliferative renal tubules and that this program is abnormally activated in proliferating cystic epithelia.

Whereas the core PCP system polarizes cells with respect to their neighbors, global directional cues are also required [18]. In the renal tubules, directional signals remain to be identified. Wnts have been proposed as directional signals in *Drosophila* [25] and in vertebrates [18], though their ability to act as instructive signals is not firmly established. Several Wnts required for kidney development [8, 13, 27, 28] should be considered as candidate directional cues. The requirement of FAT4 and DCHS1 for normal OCD suggests the possibility that these

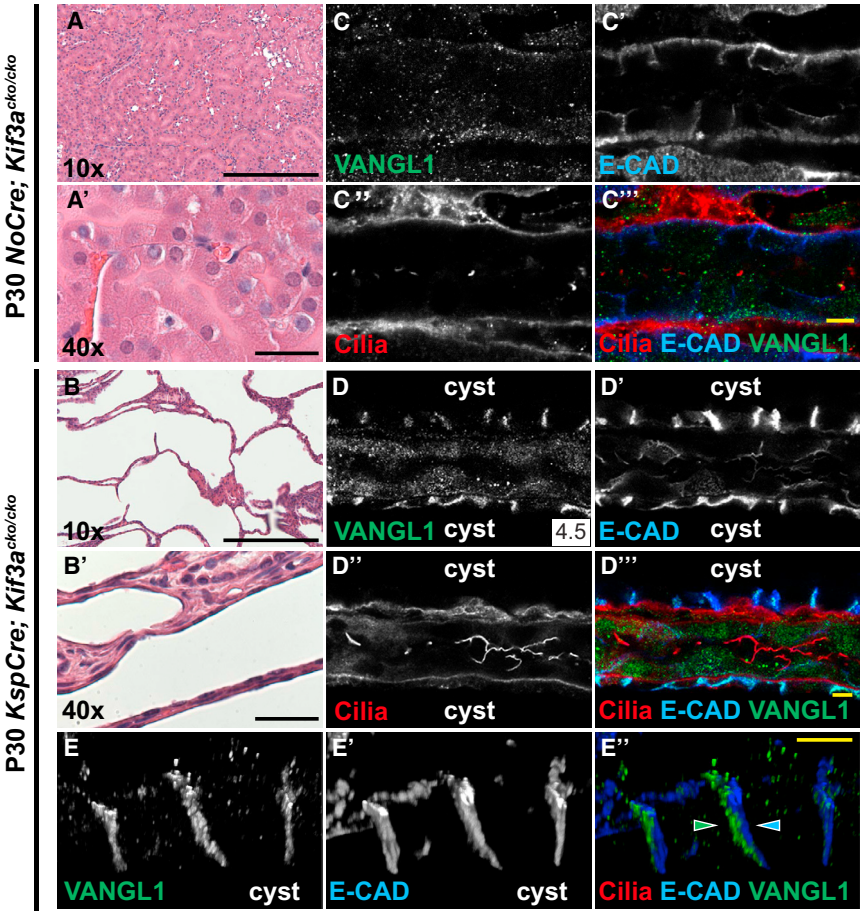

Figure 7. PCP Is Active in *Kif3a* Mutant Cystic Kidneys

(A–B') H&E-stained (A and A') P30 control (*NoCre*; *Kif3a*$^{cko/cko}$) and (B and B') *KspCre*; *Kif3a*$^{cko/cko}$ kidneys showing a strongly cystic phenotype.

(C–C'") Control P30 (*NoCre*; *Kif3a*$^{cko/cko}$) collecting duct stained for VANGL1 (green), E-CAD (blue), and acetylated α-tubulin (red; cilia).

(D–D'") *KspCre*; *Kif3a*$^{cko/cko}$ cysts stained for VANGL1 (green), E-CAD (blue), and cilia acetylated α-tubulin (red). VANGL1 signal is strong in cysts (no cilia), but not in the unaffected tubule (cilia present).

(E–E") High-magnification images from 3D reconstruction (see Movie S3) showing asymmetric localization of VANGL1 (green) relative to E-CAD (blue) in cyst-lining cells.

The scale bars represent (A–B') 200 μm and (C"', D", and E") 5 μm. See also Figure S7.

provide a directional cue analogous to that proposed for *Drosophila* Ft-Ds [11]. However, the predominantly non-epithelial expression of these proteins is not easily reconciled with this model. Further work will be required to identify global PCP directional signals in the kidney.

In renal tubules, primary cilium-associated signals are required for OCD (and likely CE) [44]. We find that intact PCP signaling is also required to correctly regulate these events. Our results are most consistent with the model that primary cilia and PCP are independently required for this regulation. PCP is intact in the absence of primary cilia, suggesting that ciliary signals regulating OCD do not act by altering PCP signaling. And whereas it is formally possible that PCP signaling acts via primary cilia to control OCD, this appears unlikely for several reasons. First, primary cilia appear to be intact in PCP mutants (data not shown). Second, PCP regulates OCD in *Drosophila* tissues that do not have primary cilia. Third, it is difficult to envision a model in which directional information from the PCP system could pass through primary cilia that do not themselves acquire a polarized localization. We therefore propose that PCP provides directional information for OCD and that a primary cilium signal is necessary to enable the response to this directional information.

By conditionally knocking out both *Vangl1* and *Vangl2* in collecting ducts, an intervention that severely disrupts core PCP signaling, we find that no cysts develop in adults up to one year of age. Therefore, disrupting PCP signaling, which in turn causes off-axis OCD and interferes with CE, does not cause cysts. Similarly, *Pkhd1*$^{del4/del4}$ mutants display off-axis OCD but do not become cystic [15]. These results imply that cilium-associated mutations that induce either prenatal or postnatal cysts must do something other than interfere with OCD and CE.

It is likely that proliferative signals fulfill this role. Loss of Kif3a induced conditionally in adult collecting ducts produced cysts only if proliferation was also induced; the induction of cysts by earlier Kif3a loss apparently requires developmentally controlled proliferation [12]. Furthermore, the cystic phenotype of *Pkd1* or *Pkd2* mutant collecting ducts (encoding polycystin-1 and -2) is suppressed by loss of cilia [45]. Removing polycystins therefore appears to activate a cilium-dependent proliferative signal for robust cystogenesis that is attenuated by disrupting cilia. Blocking PCP does not activate such a signal.

The observation that *Fat4* and *Dchs1* mutations cause dilations/cysts was suggested to support the idea that impaired PCP signaling is cystogenic [11]. However, whether or not FAT4 and DCHS1 provide PCP directional information in the kidney, the observation that *Vangl1*,*2DKO*; *Ksp-Cre* collecting ducts do not produce cysts argues against the model that FAT4 and Dachs1 act solely by disrupting core PCP signaling to induce cysts. We suggest that these mutations activate a proliferative signal. *Drosophila ft* and *ds* mutations activate Hippo signaling [46], and Hippo signaling is activated in human autosomal dominant polycystic kidney disease (ADPKD) and ARPKD [47], but Hippo signaling is not activated in FAT4- or DCHS1-associated mouse mutant dilations/cysts [33]. If *Fat4* and *Dchs1* mutations induce proliferation, this may be indirect, as the earliest indications of abnormal growth were reported to be increased cell death and decreased proliferation [33]. Of note, INTEGRIN-β1 is required for the proliferative response to *Pkd1* mutation, suggesting another possible proliferative pathway [48]. Taken together, these observations suggest that

cilium-based and non-cilium-based proliferative signals may be capable of contributing to cystogenesis.

As disrupted OCD is neither necessary nor sufficient for cystogenesis, it is unclear why it is often associated with conditions that cause cysts. One possibility is that disrupting OCD in combination with another signal is one of several distinct mechanisms of cystogenesis. This remains to be explored.

In animals ranging in size from the shrew to the elephant, proximal tubule diameters are essentially invariant [49]. Because mean arterial pressure is independent of size and therefore glomerular filtration pressure is likely also size independent, renal physiology seems to dictate an optimal diameter. One potential consequence of deviation from this optimum is variation in resistance, resulting in aberrant nephron pressure. Whereas *Vangl1*,*2*, *DKO* median diameters are larger than in wild-type, we also see some points at which diameter is smaller than wild-type, predicting that some nephrons will be subject to abnormally high pressure. Consistent with this, we observe the emergence of Bowman's space dilations consistent with type IV glomerulocystic kidney disease (GCKD) [50] in a fraction of older *Vangl1*,*2*, *DKO* animals (Figure S7; related to Figure 7; Table S1).

Our results show that PCP regulates OCD and likely CE in the renal tubules and that it is required to assure uniform tubule diameter. PCP signaling and primary cilium-associated signals appear to be independently required for maintenance of OCD. Although perturbation of OCD is frequently associated with PKD, we find that blocking PCP does not induce cysts nor is PCP disturbed in cysts induced by disruption of primary cilia. Therefore, the commonly proposed and intuitively pleasing model in which PCP is tightly associated with cystogenesis is not correct.

STAR★METHODS

Detailed methods are provided in the online version of this paper and include the following:

- KEY RESOURCES TABLE
- CONTACT FOR REAGENT AND RESOURCE SHARING
- EXPERIMENTAL MODEL AND SUBJECT DETAILS
  - Animals
- METHOD DETAILS
  - Harvesting, processing, and sectioning of kidneys
  - Antibodies and reagents
  - Immunostaining
  - Imaging
  - Tubule diameter and cell number measurements
  - Measurement of oriented cell division
  - Measurement of cell orientation
  - Quantitative real-time RT-PCR
- QUANTIFICATION AND STATISTICAL ANALYSES
  - Quantification of PCP protein asymmetry
  - Statistical analyses

SUPPLEMENTAL INFORMATION

Supplemental Information includes seven figures, two tables, and three movies and can be found with this article online at https://doi.org/10.1016/j.cub.2017.09.011.

AUTHOR CONTRIBUTIONS

Conceptualization, K.K., R.D.B., and J.D.A.; Methodology, K.K., R.D.B., E.K.V., and J.D.A.; Formal Analysis, K.K.; Investigation, K.K., R.D.B., and T.V.; Writing – Original Draft, K.K. and J.D.A.; Writing – Review & Editing, K.K., E.K.V., and J.D.A.; Funding Acquisition, K.K. and J.D.A.; Resources, E.V. and A.-R.G.; Supervision, J.D.A.

ACKNOWLEDGMENTS

We thank Jill Helms and Yingzi Yang for mice, Hao Chang and Jeremy Nathans for *Fz* mutant kidneys, Klara Fekete for help with animal husbandry, Neeraja Kambham and Andrew Connolly for pathology consults, Amarjeet Grewall and Pauline Chu for H&E staining, Daniel Gray for useful discussions, and Stefan Somlo, Greg Pazour, and Axelrod lab members for comments on the manuscript. Work was supported by a Uehara Memorial Foundation Research Fellowship and JSPS Postdoctoral Fellowships for Research Abroad (K.K.); NIH grant 5 T32 CA 9302-34 and National Kidney Foundation Postdoctoral Fellowships (R.D.B.); American Heart Association Scientist Development Grant 10SDG4590028 (A.-R.G.), NIH grants R37 GM059823 and R01 GM098582, the Stanford Child Health Research Institute, and the Stanford NIH-NCATS-CTSA (grant UL1 TR001085; J.D.A.); and the George M. O'Brien Kidney Center at Yale (NIH grant P30 DK079310).

Received: May 31, 2017
Revised: August 23, 2017
Accepted: September 7, 2017
Published: October 12, 2017

REFERENCES

1. Kagan, K.O., Dufke, A., and Gembruch, U. (2017). Renal cystic disease and associated ciliopathies. Curr. Opin. Obstet. Gynecol. *29*, 85–94.
2. Cornec-Le Gall, E., Audrézet, M.P., Le Meur, Y., Chen, J.M., and Férec, C. (2014). Genetics and pathogenesis of autosomal dominant polycystic kidney disease: 20 years on. Hum. Mutat. *35*, 1393–1406.
3. Yoder, B.K. (2007). Role of primary cilia in the pathogenesis of polycystic kidney disease. J. Am. Soc. Nephrol. *18*, 1381–1388.
4. Malicki, J.J., and Johnson, C.A. (2017). The cilium: cellular antenna and central processing unit. Trends Cell Biol. *27*, 126–140.
5. Nigro, E.A., Castelli, M., and Boletta, A. (2015). Role of the polycystins in cell migration, polarity, and tissue morphogenesis. Cells *4*, 687–705.
6. Wallingford, J.B. (2012). Planar cell polarity and the developmental control of cell behavior in vertebrate embryos. Annu. Rev. Cell Dev. Biol. *28*, 627–653.
7. Lienkamp, S.S., Liu, K., Karner, C.M., Carroll, T.J., Ronneberger, O., Wallingford, J.B., and Walz, G. (2012). Vertebrate kidney tubules elongate using a planar cell polarity-dependent, rosette-based mechanism of convergent extension. Nat. Genet. *44*, 1382–1387.
8. Karner, C.M., Chirumamilla, R., Aoki, S., Igarashi, P., Wallingford, J.B., and Carroll, T.J. (2009). Wnt9b signaling regulates planar cell polarity and kidney tubule morphogenesis. Nat. Genet. *41*, 793–799.
9. Castelli, M., Boca, M., Chiaravalli, M., Ramalingam, H., Rowe, I., Distefano, G., Carroll, T., and Boletta, A. (2013). Polycystin-1 binds Par3/aPKC and controls convergent extension during renal tubular morphogenesis. Nat. Commun. *4*, 2658.
10. Fischer, E., Legue, E., Doyen, A., Nato, F., Nicolas, J.F., Torres, V., Yaniv, M., and Pontoglio, M. (2006). Defective planar cell polarity in polycystic kidney disease. Nat. Genet. *38*, 21–23.
11. Saburi, S., Hester, I., Fischer, E., Pontoglio, M., Eremina, V., Gessler, M., Quaggin, S.E., Harrison, R., Mount, R., and McNeill, H. (2008). Loss of Fat4 disrupts PCP signaling and oriented cell division and leads to cystic kidney disease. Nat. Genet. *40*, 1010–1015.
12. Patel, V., Li, L., Cobo-Stark, P., Shao, X., Somlo, S., Lin, F., and Igarashi, P. (2008). Acute kidney injury and aberrant planar cell polarity induce cyst formation in mice lacking renal cilia. Hum. Mol. Genet. *17*, 1578–1590.

13. Yu, J., Carroll, T.J., Rajagopal, J., Kobayashi, A., Ren, Q., and McMahon, A.P. (2009). A Wnt7b-dependent pathway regulates the orientation of epithelial cell division and establishes the cortico-medullary axis of the mammalian kidney. Development *136*, 161–171.
14. Luyten, A., Su, X., Gondela, S., Chen, Y., Rompani, S., Takakura, A., and Zhou, J. (2010). Aberrant regulation of planar cell polarity in polycystic kidney disease. J. Am. Soc. Nephrol. *21*, 1521–1532.
15. Nishio, S., Tian, X., Gallagher, A.R., Yu, Z., Patel, V., Igarashi, P., and Somlo, S. (2010). Loss of oriented cell division does not initiate cyst formation. J. Am. Soc. Nephrol. *21*, 295–302.
16. Jonassen, J.A., SanAgustin, J., Baker, S.P., and Pazour, G.J. (2012). Disruption of IFT complex A causes cystic kidneys without mitotic spindle misorientation. J. Am. Soc. Nephrol. *23*, 641–651.
17. Brzóska, H.L., d'Esposito, A.M., Kolatsi-Joannou, M., Patel, V., Igarashi, P., Lei, Y., Finnell, R.H., Lythgoe, M.F., Woolf, A.S., Papakrivopoulou, E., and Long, D.A. (2016). Planar cell polarity genes Celsr1 and Vangl2 are necessary for kidney growth, differentiation, and rostrocaudal patterning. Kidney Int. *90*, 1274–1284.
18. Vladar, E.K., Antic, D., and Axelrod, J.D. (2009). Planar cell polarity signaling: the developing cell's compass. Cold Spring Harb. Perspect. Biol. *1*, a002964.
19. Tree, D.R., Ma, D., and Axelrod, J.D. (2002). A three-tiered mechanism for regulation of planar cell polarity. Semin. Cell Dev. Biol. *13*, 217–224.
20. Tree, D.R., Shulman, J.M., Rousset, R., Scott, M.P., Gubb, D., and Axelrod, J.D. (2002). Prickle mediates feedback amplification to generate asymmetric planar cell polarity signaling. Cell *109*, 371–381.
21. Amonlirdviman, K., Khare, N.A., Tree, D.R., Chen, W.S., Axelrod, J.D., and Tomlin, C.J. (2005). Mathematical modeling of planar cell polarity to understand domineering nonautonomy. Science *307*, 423–426.
22. Butler, M.T., and Wallingford, J.B. (2017). Planar cell polarity in development and disease. Nat. Rev. Mol. Cell Biol. *18*, 375–388.
23. Matis, M., and Axelrod, J.D. (2013). Regulation of PCP by the Fat signaling pathway. Genes Dev. *27*, 2207–2220.
24. Sharp, K.A., and Axelrod, J.D. (2016). Prickle isoforms control the direction of tissue polarity by microtubule independent and dependent mechanisms. Biol. Open *5*, 229–236.
25. Wu, J., Roman, A.C., Carvajal-Gonzalez, J.M., and Mlodzik, M. (2013). Wg and Wnt4 provide long-range directional input to planar cell polarity orientation in *Drosophila*. Nat. Cell Biol. *15*, 1045–1055.
26. Tissir, F., and Goffinet, A.M. (2013). Shaping the nervous system: role of the core planar cell polarity genes. Nat. Rev. Neurosci. *14*, 525–535.
27. Huang, L., Xiao, A., Wecker, A., McBride, D.A., Choi, S.Y., Zhou, W., and Lipschutz, J.H. (2014). A possible zebrafish model of polycystic kidney disease: knockdown of wnt5a causes cysts in zebrafish kidneys. J. Vis. Exp. (94), 52156.
28. Nagy, I.I., Xu, Q., Naillat, F., Ali, N., Miinalainen, I., Samoylenko, A., and Vainio, S.J. (2016). Impairment of Wnt11 function leads to kidney tubular abnormalities and secondary glomerular cystogenesis. BMC Dev. Biol. *16*, 30.
29. Otto, E.A., Schermer, B., Obara, T., O'Toole, J.F., Hiller, K.S., Mueller, A.M., Ruf, R.G., Hoefele, J., Beekmann, F., Landau, D., et al. (2003). Mutations in INVS encoding inversin cause nephronophthisis type 2, linking renal cystic disease to the function of primary cilia and left-right axis determination. Nat. Genet. *34*, 413–420.
30. Germino, G.G. (2005). Linking cilia to Wnts. Nat. Genet. *37*, 455–457.
31. Rock, R., Schrauth, S., and Gessler, M. (2005). Expression of mouse dchs1, fjx1, and fat-j suggests conservation of the planar cell polarity pathway identified in *Drosophila*. Dev. Dyn. *234*, 747–755.
32. Ishiuchi, T., Misaki, K., Yonemura, S., Takeichi, M., and Tanoue, T. (2009). Mammalian Fat and Dachsous cadherins regulate apical membrane organization in the embryonic cerebral cortex. J. Cell Biol. *185*, 959–967.
33. Mao, Y., Mulvaney, J., Zakaria, S., Yu, T., Morgan, K.M., Allen, S., Basson, M.A., Francis-West, P., and Irvine, K.D. (2011). Characterization of a Dchs1 mutant mouse reveals requirements for Dchs1-Fat4 signaling during mammalian development. Development *138*, 947–957.
34. Yates, L.L., Papakrivopoulou, J., Long, D.A., Goggolidou, P., Connolly, J.O., Woolf, A.S., and Dean, C.H. (2010). The planar cell polarity gene Vangl2 is required for mammalian kidney-branching morphogenesis and glomerular maturation. Hum. Mol. Genet. *19*, 4663–4676.
35. Park, T.J., Mitchell, B.J., Abitua, P.B., Kintner, C., and Wallingford, J.B. (2008). Dishevelled controls apical docking and planar polarization of basal bodies in ciliated epithelial cells. Nat. Genet. *40*, 871–879.
36. Cao, Y., Park, A., and Sun, Z. (2010). Intraflagellar transport proteins are essential for cilia formation and for planar cell polarity. J. Am. Soc. Nephrol. *21*, 1326–1333.
37. Ehaideb, S.N., Iyengar, A., Ueda, A., Iacobucci, G.J., Cranston, C., Bassuk, A.G., Gubb, D., Axelrod, J.D., Gunawardena, S., Wu, C.F., and Manak, J.R. (2014). prickle modulates microtubule polarity and axonal transport to ameliorate seizures in flies. Proc. Natl. Acad. Sci. USA *111*, 11187–11192.
38. Wang, Y., Guo, N., and Nathans, J. (2006). The role of Frizzled3 and Frizzled6 in neural tube closure and in the planar polarity of inner-ear sensory hair cells. J. Neurosci. *26*, 2147–2156.
39. Yin, H., Copley, C.O., Goodrich, L.V., and Deans, M.R. (2012). Comparison of phenotypes between different vangl2 mutants demonstrates dominant effects of the Looptail mutation during hair cell development. PLoS ONE *7*, e31988.
40. Lin, F., Hiesberger, T., Cordes, K., Sinclair, A.M., Goldstein, L.S., Somlo, S., and Igarashi, P. (2003). Kidney-specific inactivation of the KIF3A subunit of kinesin-II inhibits renal ciliogenesis and produces polycystic kidney disease. Proc. Natl. Acad. Sci. USA *100*, 5286–5291.
41. Wallingford, J.B., and Mitchell, B. (2011). Strange as it may seem: the many links between Wnt signaling, planar cell polarity, and cilia. Genes Dev. *25*, 201–213.
42. Jones, C., Roper, V.C., Foucher, I., Qian, D., Banizs, B., Petit, C., Yoder, B.K., and Chen, P. (2008). Ciliary proteins link basal body polarization to planar cell polarity regulation. Nat. Genet. *40*, 69–77.
43. Guirao, B., Meunier, A., Mortaud, S., Aguilar, A., Corsi, J.M., Strehl, L., Hirota, Y., Desoeuvre, A., Boutin, C., Han, Y.G., et al. (2010). Coupling between hydrodynamic forces and planar cell polarity orients mammalian motile cilia. Nat. Cell Biol. *12*, 341–350.
44. Costantini, F., and Kopan, R. (2010). Patterning a complex organ: branching morphogenesis and nephron segmentation in kidney development. Dev. Cell *18*, 698–712.
45. Ma, M., Tian, X., Igarashi, P., Pazour, G.J., and Somlo, S. (2013). Loss of cilia suppresses cyst growth in genetic models of autosomal dominant polycystic kidney disease. Nat. Genet. *45*, 1004–1012.
46. Sharma, P., and McNeill, H. (2013). Fat and Dachsous cadherins. Prog. Mol. Biol. Transl. Sci. *116*, 215–235.
47. Happé, H., van der Wal, A.M., Leonhard, W.N., Kunnen, S.J., Breuning, M.H., de Heer, E., and Peters, D.J. (2011). Altered Hippo signalling in polycystic kidney disease. J. Pathol. *224*, 133–142.
48. Lee, K., Boctor, S., Barisoni, L.M., and Gusella, G.L. (2015). Inactivation of integrin-β1 prevents the development of polycystic kidney disease after the loss of polycystin-1. J. Am. Soc. Nephrol. *26*, 888–895.
49. Calder, W.A., 3rd, and Braun, E.J. (1983). Scaling of osmotic regulation in mammals and birds. Am. J. Physiol. *244*, R601–R606.
50. Lennerz, J.K., Spence, D.C., Iskandar, S.S., Dehner, L.P., and Liapis, H. (2010). Glomerulocystic kidney: one hundred-year perspective. Arch. Pathol. Lab. Med. *134*, 583–605.
51. Vladar, E.K., Bayly, R.D., Sangoram, A.M., Scott, M.P., and Axelrod, J.D. (2012). Microtubules enable the planar cell polarity of airway cilia. Curr. Biol. *22*, 2203–2212.

52. Antic, D., Stubbs, J.L., Suyama, K., Kintner, C., Scott, M.P., and Axelrod, J.D. (2010). Planar cell polarity enables posterior localization of nodal cilia and left-right axis determination during mouse and Xenopus embryogenesis. PLoS ONE *5*, e8999.

53. Song, H., Hu, J., Chen, W., Elliott, G., Andre, P., Gao, B., and Yang, Y. (2010). Planar cell polarity breaks bilateral symmetry by controlling ciliary positioning. Nature *466*, 378–382.

54. Gallagher, A.R., Esquivel, E.L., Briere, T.S., Tian, X., Mitobe, M., Menezes, L.F., Markowitz, G.S., Jain, D., Onuchic, L.F., and Somlo, S. (2008). Biliary and pancreatic dysgenesis in mice harboring a mutation in Pkhd1. Am. J. Pathol. *172*, 417–429.

55. Igarashi, P., Shashikant, C.S., Thomson, R.B., Whyte, D.A., Liu-Chen, S., Ruddle, F.H., and Aronson, P.S. (1999). Ksp-cadherin gene promoter. II. Kidney-specific activity in transgenic mice. Am. J. Physiol. *277*, F599–F610.

STAR★METHODS

KEY RESOURCES TABLE

REAGENT or RESOURCE	SOURCE	IDENTIFIER
Antibodies		
Rabbit anti-Vangl1	Sigma-Aldrich	HPA025235
Rabbit anti-Vangl2	Millipore	ABN373
Goat anti-Frizzled6	R&D Systems	AF1526
Goat anti-Frizzled3	R&D Systems	AF1001
Rat anti-Frizzled3	R&D Systems	MAB1001
Rat anti-E-Cadherin	Thermo Fisher Scientific	131900
Mouse anti-E-cadherin	BD Transduction Laboratories	610181
Mouse anti-acetylated-α-tubulin	Sigma-Aldrich	6-11B-1
Rabbit anti-phospho-Histone H3 (Ser10)	Millipore	06-570
Mouse anti-β-catenin	BD Transduction Laboratories	610153
Goat anti-AQP2	Santa Cruz Biotechnology	SC-9882
Alexa 488 donkey-anti-rabbit	Thermo Fisher Scientific	A-21206
Alexa 594 donkey-anti-rabbit	Thermo Fisher Scientific	A-21207
Alexa 488 donkey-anti-goat	Thermo Fisher Scientific	A-11055
Alexa 546 donkey-anti-goat	Thermo Fisher Scientific	A-11056
Alexa 594 donkey-anti-rat	Thermo Fisher Scientific	A-21209
Alexa 633 goat-anti-rat	Thermo Fisher Scientific	A-21094
Alexa 647 chicken-anti-rat	Thermo Fisher Scientific	A-21472
Alexa 647 donkey-anti-mouse	Thermo Fisher Scientific	A-31571
Phalloidin conjugated to Alexa 635	Thermo Fisher Scientific	A-34054
Streptavidin conjugated to Alexa 488	Thermo Fisher Scientific	S-32354
Streptavidin conjugated to Alexa 594	Thermo Fisher Scientific	S-32356
Fluorescein-conjugated *Lotus Tetragonolobus* lectin (LTL)	Vector Laboratories	FL-1321
Biotinylated *Lotus Tetragonolobus* lectin (LTL)	Vector Laboratories	B-1325
Rhodamine-conjugated *Dolichos Biflorus Agglutinin* (DBA)	Vector Laboratories	RL-1032
DAPI	Sigma-Aldrich	D-9542
Sytox Green (1:20,000, Invitrogen)	Thermo Fisher Scientific	S7020
7-aminoactinomycin D (7-AAD, 1:40, Invitrogen)	Thermo Fisher Scientific	A1310
Critical Commercial Assays		
QIAGEN RNeasy Mini Kit	QIAGEN	74104
SuperScript III 1st Strand cDNA Synthesis Kit	Thermo Fisher Scientific	18080051
Power SYBR Green PCR Master Mix	Thermo Fisher Scientific	4367659
Applied Biosystems StepOnePlus Real-Time PCR System	Applied Biosystems	4376592R
Experimental Models: Organisms/Strains		
Vangl1$^{cko/cko}$ mouse	Created in our lab [51]	N/A
Vangl1$^{-/-}$ (previously referred to as *Vangl1CKO*$^{\Delta/\Delta}$) mouse	Created in our lab [52]	N/A
Vangl2$^{Lp/Lp}$ mouse	The Jackson Laboratory	JAX: 000220
Vangl2$^{cko/cko}$ mouse	Gift from Y. Yang [53]	N/A
Kif3a$^{cko/cko}$ mouse	Gift from J. Helms [40]	N/A
Ksp-Cre mouse	Gift from The George M. O'Brien Kidney Center [40]	N/A
Fz3$^{-/-}$;*Fz6*$^{-/-}$ mouse kidney samples	Gift from H. Chang and J. Nathans [38]	N/A
Pkhd1$^{del4/del4}$ mouse kidney samples	Gift from The George M. O'Brien Kidney Center [54]	N/A

(*Continued on next page*)

Continued		
REAGENT or RESOURCE	SOURCE	IDENTIFIER
Oligonucleotides		
See Table S2 for oligonucleotides for qRT-PCR	Stanford PAN facility	N/A
Software and Algorithms		
GraphPad Prism	GraphPad Software	https://www.graphpad.com/scientific-software/prism/
ImageJ	NIH	https://imagej.nih.gov/ij/

CONTACT FOR REAGENT AND RESOURCE SHARING

Further information and requests for resources and reagents should be directed to and will be fulfilled by the Lead Contact, Jeff Axelrod (jaxelrod@stanford.edu).

EXPERIMENTAL MODEL AND SUBJECT DETAILS

Animals

Vangl1$^{-/-}$ (previously referred to as *Vangl1*$^{cko/cko}$) [51], *KspCre;Kif3a*$^{cko/cko}$ [40], *Fz3*$^{-/-}$*;Fz6*$^{-/-}$ [38], *Vangl2*$^{cko/cko}$ [53], *Pkhd1*$^{del4/del4}$ [15] and *Vl2*$^{Lp/Lp}$ (JAX) mice and genotyping have been previously described. *KspCre*; *Vangl1*$^{cko/cko}$; *Vangl2*$^{cko/cko}$ (*Vangl1,2*, *DKO*, *Ksp-Cre*) animals were bred from heterozygotes. KspCre drives Cre expression beginning in the early branching ureteric bud stage [55]. Animals were healthy with normal immune status, were not subject to prior procedures, were drug naive and were reared by standard husbandry and housed in standard cages in the Stanford Animal Care Facility. Approximately equal numbers of animals of either sex were used for all experiments. Specimens were collected at the ages indicated in text and legends. All procedures involving animals were approved by the Stanford University Institutional Animal Care and Use Committee in accordance with established guidelines for animal care.

METHOD DETAILS

Harvesting, processing, and sectioning of kidneys

For dehydration fixation, postnatal and embryonic kidneys (E13.5 – E18.5) were harvested and sub dissected in PBS. Collected kidneys were then placed in 4% paraformaldehyde in PBS for 1 hr and transferred into a 30% sucrose solution in calcium and magnesium free PBS at 4°C overnight. The following day, the kidneys were submerged in OCT mounting media and frozen in blocks in an ethanol and dry ice bath and could be stored for further use at −80°C. 12 – 20 μμ sections through kidneys were made using a Leica CM 3050S cryostat and mounted on charged slides.

For standard fixation, kidneys were harvested and sub dissected in OCT mounting media and frozen in blocks in liquid nitrogen. The samples could be stored for further use at −80°C. 10 – 30 μμ sections through kidneys were made using a Leica CM 3050S cryostat and mounted on charged slides. Samples were fixed in 3.7% formaldehyde or 4% paraformaldehyde in PBS for 10 min and soaked in 0.2% Triton X-100 in PBS for 5 min prior to immunostaining.

For hematoxylin and eosin (H&E) staining, kidneys were fixed in 4% paraformaldehyde in PBS for 1 hr, then in 70% ethanol for 12 hr prior to paraffin-embedding. Paraffin blocks were sectioned at 4 μμ thickness and stained with H&E.

Antibodies and reagents

The dilution and sources for primary antibodies used were as follows: rabbit anti-Vangl1 (1:200, Sigma), rabbit anti-VANGL2 (1:200, Santa Cruz), goat anti-FRIZZLED6 (1:200, R&D Systems), goat anti-FRIZZLED3 (1:100, R&D Systems), rat anti-FRIZZLED3 (1:100, R&D Systems), rat anti-E-CADHERIN (1:200, Invitrogen) and mouse anti-E-CADHERIN (1:200, BD Transduction Laboratories), mouse anti-acetylated-α-TUBULIN (1:500, Sigma), rabbit anti-phospho-HISTONE H3 (Ser10) (1:200, Millipore) and mouse anti-β-CATENIN (1:100, BD Transduction Laboratories). The following secondary antibodies were used at 1:500 and purchased from Molecular Probes (now ThermoFisher): Alexa 488, 594 donkey-anti-rabbit, Alexa 488, 546 donkey-anti-goat, Alexa 594, 633 donkey-anti-rat, Alexa 647 chicken-anti-rat and STREPTAVIDIN Alexa 594 conjugate. PHALLOIDIN conjugated to Alexa 633 was used at 1:50. RHODAMINE-conjugated *Dolichos Biflorus Agglutinin* lectin (DBA, 1:50, Vector Laboratories) and goat anti-AQP2 (1:200, Santa Cruz) were used to stain collecting duct. FLUORESCEIN-conjugated *Lotus Tetragonolobus* lectin (LTL, 1:200, Vector Laboratories) and biotinylated *Lotus Tetragonolobus* lectin (1:200, Vector Laboratories) were used to stain proximal tubules. DAPI (300nM, Sigma), Sytox Green (1:20,000, Invitrogen) and 7-aminoactinomycin D (7-AAD, 1:40, Invitrogen) were used to stain nuclei.

Immunostaining

Immunostaining was done according to the following steps:

1. 3x 10min wash in PBT (Phosphate Buffered Saline [PBS] + 0.1% Triton X-100)
2. 1 hr incubation in PBT +10% normal horse serum (NHS) or 1% BSA in PBS
3. Overnight incubation with primary antibodies at required dilution in PBT +10% NHS
4. Next day, 3x 10min wash in PBT
5. 1 hr incubation with secondary antibodies at required dilution in PBT +10% NHS
6. 3x 10 min wash in PBT
7. Add mounting media and apply coverslip

Imaging

For immunofluorescence, sections were mounted in ProLong® Gold Antifade Reagent (Invitrogen) or Vectashield® (Vector Laboratories) mounting medium. Specimens were imaged with a Leica SP5 or SP8 confocal microscope, using accompanying acquisition and 3D software. For bright field, kidneys were imaged with a Nikon Eclipse E1000M microscope and acquired using Spot imaging software.

Tubule diameter and cell number measurements

To measure the diameter of kidney tubules, we stained collecting duct (DBA or AQP2) and proximal tubules (LTL), together with E-CAD. Branching tubules were avoided and we limited our analysis to tubules that were roughly circular in cross-section [8]. To compensate for obliqueness of section, the shortest diameter was measured using ImageJ or Leica software. For consistency, collecting duct diameter was measured in the cortex and proximal medulla near the corticomedullary junction. Due to non-Gaussian distributions, medians were calculated and significance determined by the Mann-Whitney U test. The number of cells within the cross-section of kidney tubules was measured in a similar manner, using (1:20,000, Invitrogen) and 7-aminoactinomycin D (7-AAD, 1:40, Invitrogen) to label nuclei. Nuclei were manually counted in ImageJ. Data are reported as mean ± SEM. Measurements could not be performed in a blinded fashion, as the genotypes are readily recognizable. To address this, for many of the conditions, measurements were performed independently by two different individuals; good concordance between the independent results was achieved.

Measurement of oriented cell division

The method for measuring orientation of mitotic angles was adopted and modified from [10]. Kidney sections (30 μ thick) were stained with anti-phospho-HISTONE H3 (Ser10) antibody to label the chromosomes of dividing cells in late anaphase and telophase. Sections were co-stained with anti-AQP2 or DBA to label the tubular apical membranes. Z stack images were acquired by confocal microscopy. The orientation of cell division was determined by measuring the angle between the mitotic spindles of dividing cells and the longitudinal axis of the collecting ducts. Angular distributions were visualized by rose diagram using Oriana software.

Measurement of cell orientation

The orientation of cells was measured in the collecting duct and proximal tubules of kidneys from E15.5 - E18.5 similar to previous reports [8]. For cell orientation analysis, 20 μμ kidney sections were stained for DBA, LTL and E-CAD. Confocal Z stacks were captured through entire tubules to ensure that branching tubules were avoided. From these Z stacks, the outlines of cells, demarcated by E-CAD staining, immediately below the apical (luminal) surface were traced using ImageJ (NIH). Cells that shared an edge with the outside of the tubule in our images were excluded from analysis. The software then calculated the length of the long and short axes and the angle of the long axis for each cell. We limited our analyses of cell orientation to cells that possessed a length:width ratio greater than 1.2 [8]. The angle of orientation for each cell was calculated as the difference between angle of the long axis of each cell and the angle of the tubule segment from which it is a part of. The data was visualized in histograms by graphing the percentage of events in 10° bins.

Quantitative real-time RT-PCR

Total RNA was isolated from 3 P1 kidneys and 3 16w kidneys using the QIAGEN RNeasy Mini Kit (QIAGEN, Valencia, CA). cDNA was generated with the SuperScript III 1st Strand cDNA Synthesis Kit (Life Technologies, Carlsbad, CA). Quantitative realtime PCR was performed in triplicate with SYBR GreenER qPCR SuperMix for ABI PRISM (Life Technologies, Carlsbad, CA) in an Applied Biosystems StepOnePlus Real-Time PCR System (Applied Biosystems, Foster City, CA) using the primers in Table S2. PCR was performed for 40 cycles of 95°C for 15 s and 60°C for 60 s.

QUANTIFICATION AND STATISTICAL ANALYSES

Quantification of PCP protein asymmetry

Samples prepared by the dehydration method were double labeled with either E-CAD or β-CATENIN and the PCP protein of interest. At cell-cell junctions that were separated by dehydration, regions encompassing proximal and distal membranes as defined by the

E-CAD or β-CATENIN staining were defined using ImageJ software, and average pixel intensity was recorded. On average, the proximal and distal intensities were approximately equal for E-CAD and β-CATENIN. The same regions were then used to measure intensities in the PCP channel. PCP intensities were normalized to the corresponding E-CAD or β-CATENIN measurements, and the ratio of proximal to distal (Vang) or distal to proximal (Fz) of the normalized values was determined. The average intensity ratio (IR) for each PCP protein was then determined and reported in the associated Figure panel and graphically ± SEM in Figure S3. We used a minimum of 10 well imaged and separated proximal-distal junctions, and in most cases more for each condition, except for the E13.5 measurements (n = 8 for Vangl1 and n = 5 for FZ6).

Statistical analyses

The Mann-Whitney U test was used to determine significance of difference in median measurements due to the non-Gaussian distribution of datasets.

Current Biology, Volume *27*

Supplemental Information

Disruption of Core Planar Cell Polarity Signaling Regulates Renal Tubule Morphogenesis but Is Not Cystogenic

Koshi Kunimoto, Roy D. Bayly, Eszter K. Vladar, Tyson Vonderfecht, Anna-Rachel Gallagher, and Jeffrey D. Axelrod

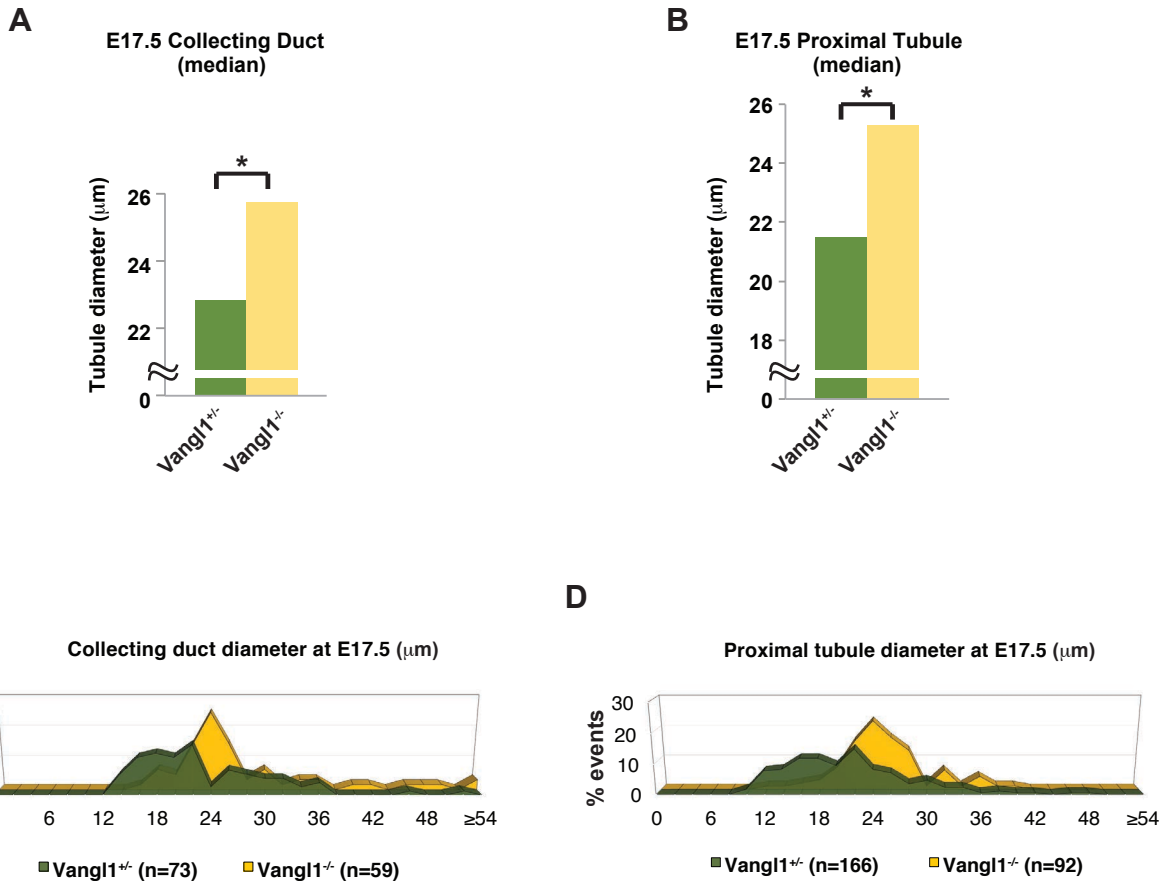
A
E17.5 Collecting Duct
(median)
Tubule diameter (μm)
26
24
22
0
*
Vangl1+/-
Vangl1-/-
B
E17.5 Proximal Tubule
(median)
Tubule diameter (μm)
26
24
22
20
18
0
*
Vangl1+/-
Vangl1-/-
C
Collecting duct diameter at E17.5 (μm)
% events
30
20
10
0
0
6
12
18
24
30
36
42
48
≥54
Vangl1+/- (n=73)
Vangl1-/- (n=59)
D
Proximal tubule diameter at E17.5 (μm)
% events
30
20
10
0
0
6
12
18
24
30
36
42
48
≥54
Vangl1+/- (n=166)
Vangl1-/- (n=92)

Figure S1. *Vangl1* mutant tubule diameters are enlarged at E17.5. Related to Figure 1.

Median collecting duct (A) and proximal tubule (B) diameters in control (*Vangl1*$^{+/-}$) and *Vangl1*$^{-/-}$ mutant kidneys. * = $p<0.0001$ by Mann-Whitney U test). (C-D) Distribution of diameters from (A) and (B), respectively. Measurements made using the low calcium dehydration method.

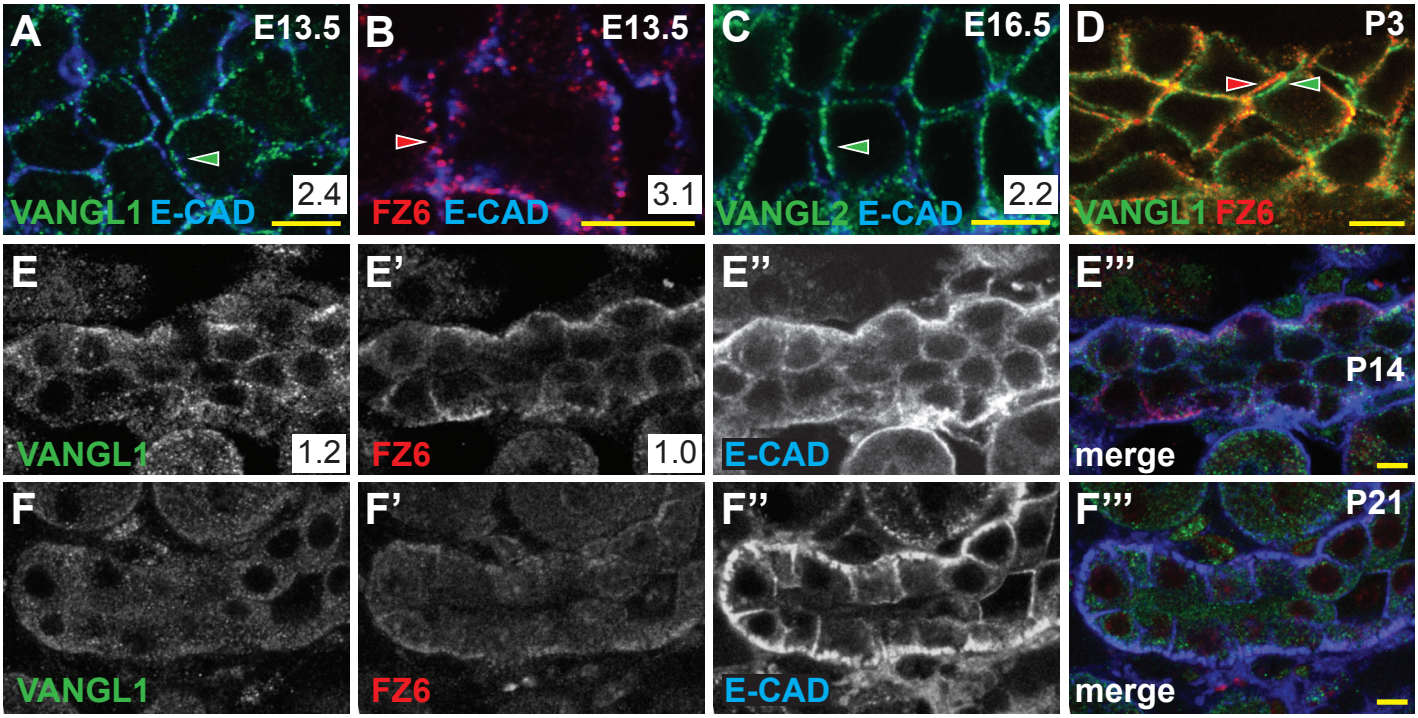
A
E13.5
VANGL1 E-CAD
2.4
B
E13.5
FZ6 E-CAD
3.1
C
E16.5
VANGL2 E-CAD
2.2
D
P3
VANGL1 FZ6
E
VANGL1
1.2
E'
FZ6
1.0
E''
E-CAD
E'''
P14
merge
F
VANGL1
F'
FZ6
F''
E-CAD
F'''
P21
merge

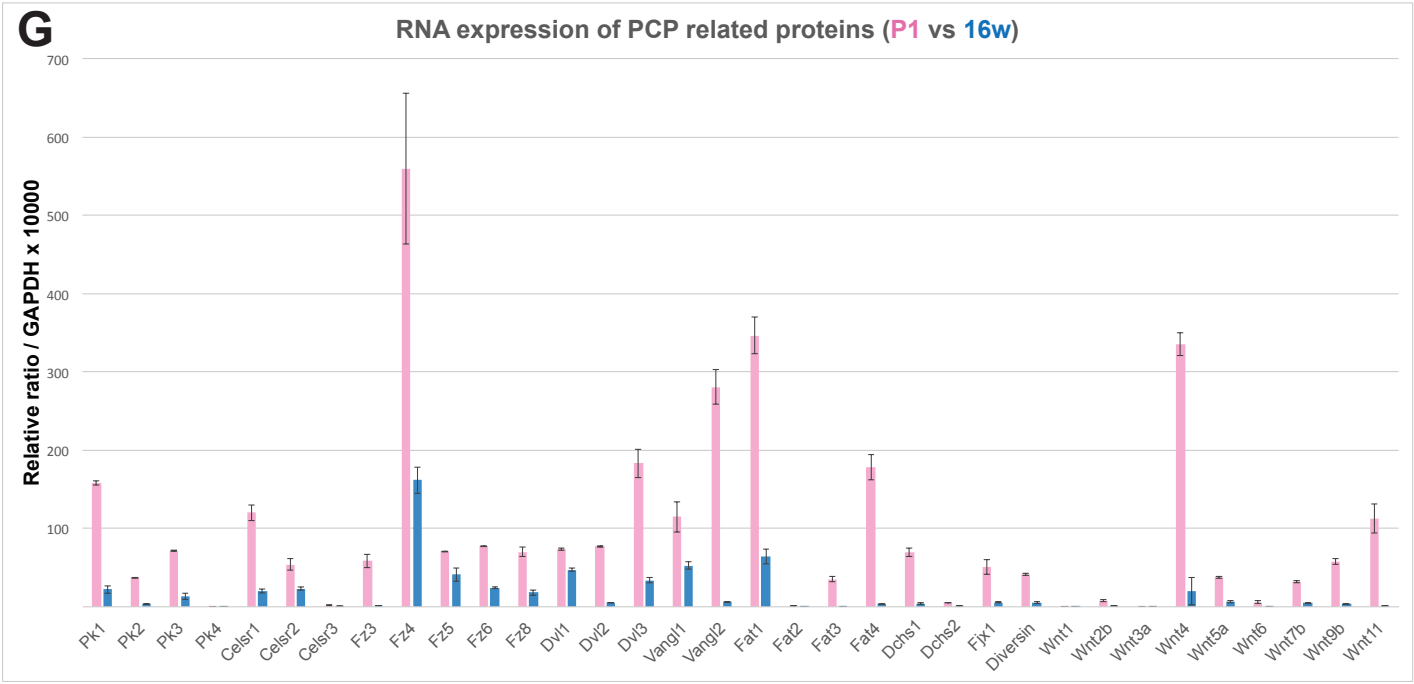
G
RNA expression of PCP related proteins (P1 vs 16w)
Relative ratio / GAPDH x 10000
700
600
500
400
300
200
100
Pk1
Pk2
Pk3
Pk4
Celsr1
Celsr2
Celsr3
Fz3
Fz4
Fz5
Fz6
Fz8
Dvl1
Dvl2
Dvl3
Vangl1
Vangl2
Fat1
Fat2
Fat3
Fat4
Dchs1
Dchs2
Fjx1
Diversin
Wnt1
Wnt2b
Wnt3a
Wnt4
Wnt5a
Wnt6
Wnt7b
Wnt9b
Wnt11

Figure S2. Embryonic PCP protein asymmetric localization and expression declines postnatally. Related to Figure 2. (A-F) Collecting ducts from WT kidneys stained for VANGL1 (green), VANGL2 (green) or FZ6 (red) and E-CAD (blue) from age E13.5 to P21. Asymmetric VANGL1 and FZ6 localization are seen throughout embryonic stages and through P3. Membrane associated staining of PCP proteins declines after P3, with some residual membrane associated signal and mostly cytoplasmic signal evident at P15. By P21, minimal membrane associated signal remains. See also Figure 7 for comparable P30 images. (G) qPCR of PCP and related genes, normalized to GAPDH, at P1 and 16 weeks shows decreased gene expression over this time span. Error bars are SEM for n=3 measurements. Scale bars: 5 μm.

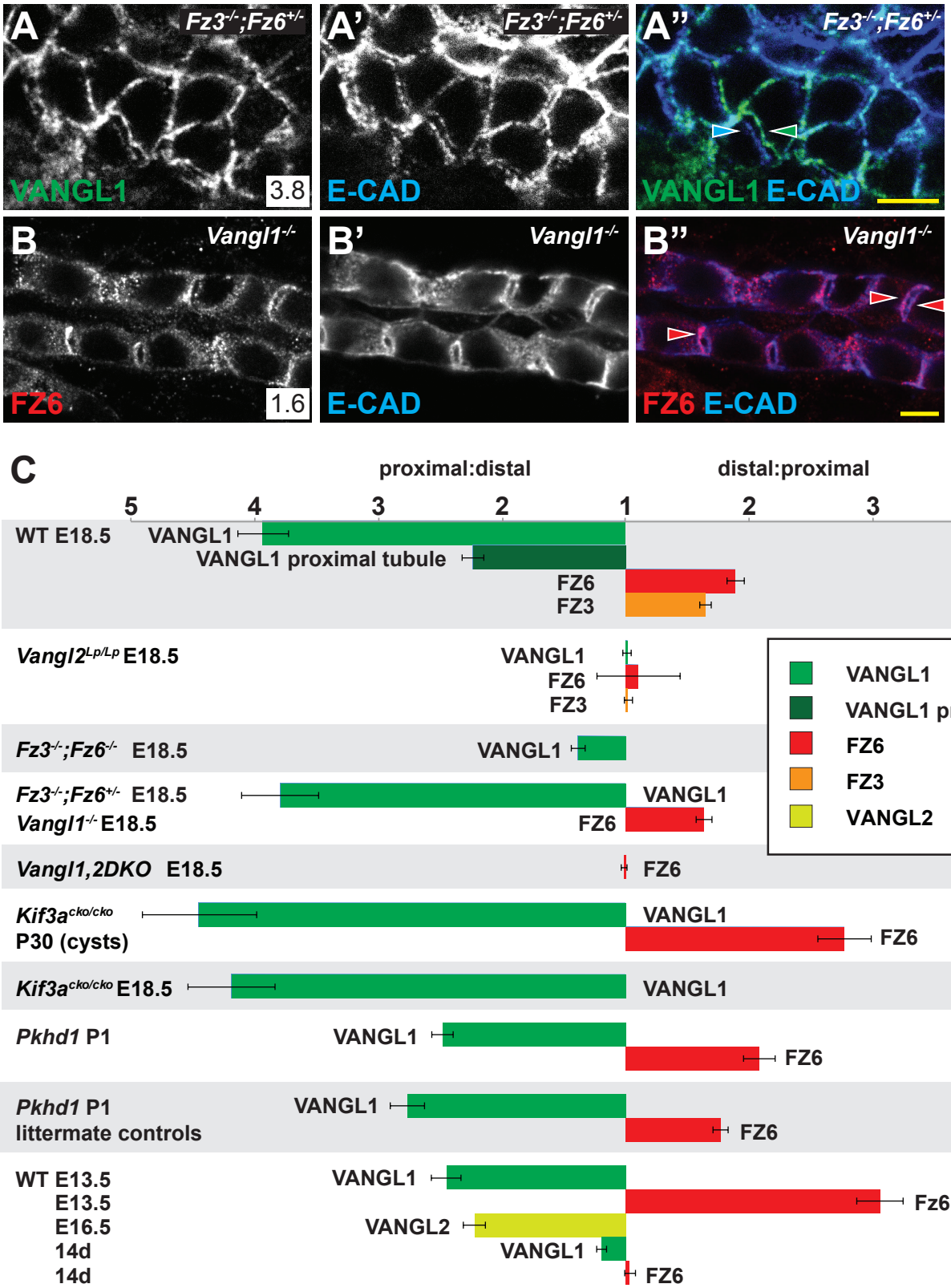
A
Fz3-/-;Fz6+/-
VANGL1
3.8
A'
Fz3-/-;Fz6+/-
E-CAD
A''
Fz3-/-;Fz6+/-
VANGL1 E-CAD
B
Vangl1-/-
FZ6
1.6
B'
Vangl1-/-
E-CAD
B''
Vangl1-/-
FZ6 E-CAD
C
proximal:distal
distal:proximal
5
4
3
2
1
2
3
4
WT E18.5
VANGL1
VANGL1 proximal tubule
FZ6
FZ3
Vangl2Lp/Lp E18.5
VANGL1
FZ6
FZ3
Fz3-/-;Fz6-/- E18.5
VANGL1
Fz3-/-;Fz6+/- E18.5
Vangl1-/- E18.5
VANGL1
FZ6
Vangl1,2DKO E18.5
FZ6
Kif3acko/cko
P30 (cysts)
VANGL1
FZ6
Kif3acko/cko E18.5
VANGL1
Pkhd1 P1
VANGL1
FZ6
Pkhd1 P1
littermate controls
VANGL1
FZ6
WT E13.5
E13.5
E16.5
14d
14d
VANGL1
Fz6
VANGL2
VANGL1
FZ6
VANGL1
VANGL1 prox
FZ6
FZ3
VANGL2

Figure S3. Asymmetric localization of core PCP protein localization in E18.5 PCP mutants. Related to Figure 3. (A-A'') VANGL1 (green) and E-CAD (blue) in *Fz3*$^{-/-}$*; Fz6*$^{+/-}$ kidneys. One copy of *Fz6* is sufficient to support PCP signaling as assessed by VANGL1 asymmetric localization. (B-B'') FZ6 (red) and E-CAD (blue) in a *Vangl1*$^{-/-}$ mutant collecting duct. Asymmetric localization of FZ6 is modestly diminished though not lost. Scale bars: 5 μm. (C) Graph of Intensity Ratios (IRs) representing asymmetry of core PCP protein distributions for conditions examined throughout the manuscript. All values are for collecting ducts unless marked otherwise. Ratios are shown ± SEM. See STAR Methods for method of measurement.

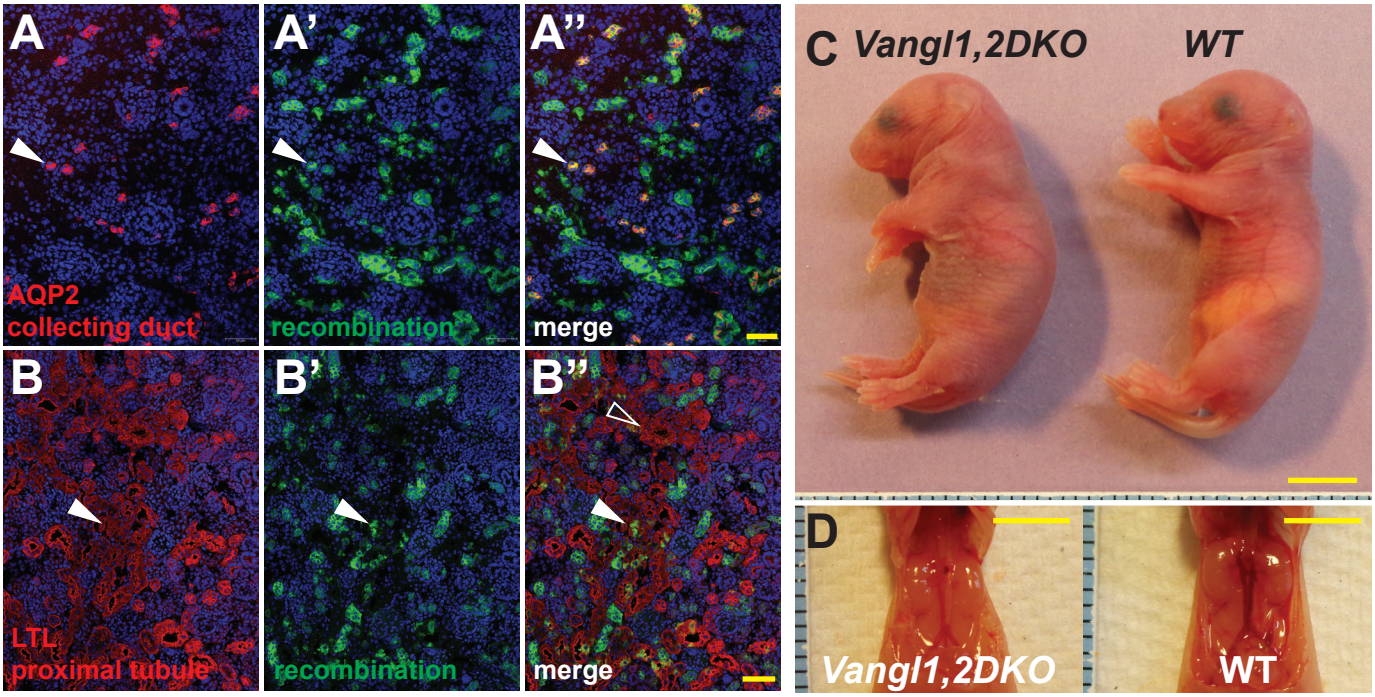

Low calcium dehydration method

E Collecting duct diameter at E18.5 (μm)

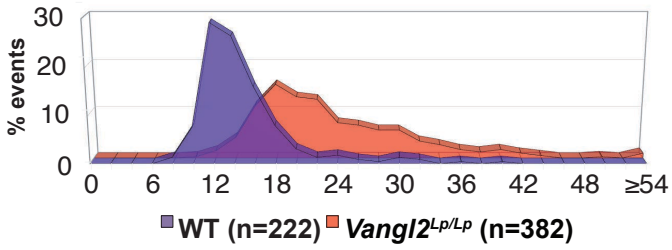

F Proximal tubule diameter at E18.5 (μm)

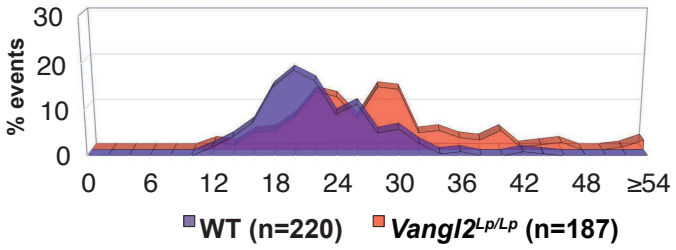

Standard fixation method

G Collecting duct diameter at E18.5 (μm)

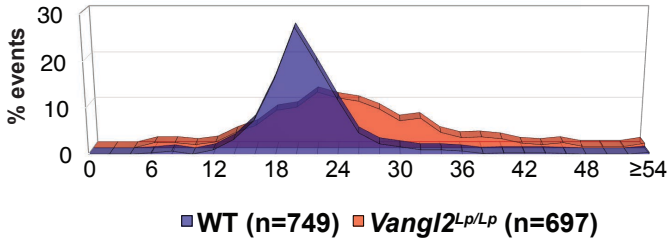

H Proximal tubules diameter at E18.5 (μm)

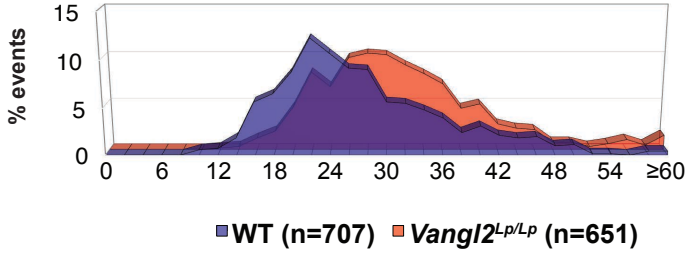

Figure S4. Validation of the *Vangl1,2 DKO* mutant kidneys. Related to Figure 4. The mTmG reporter [S1] in *P1 Vangl1,2DKO* kidneys stained for AQP2 (A-A''; red; collecting duct) or LTL (B-B''; red; proximal tubules) and DAPI (blue) showing only the GFP (green) signal from mTmG indicating recombination. Virtually all collecting duct cells display recombination, and a small number of proximal tubule cells show recombination. (C-D) Gross views of *VangL1,2DKO* and control mice and kidneys. (E-H) Comparison of the low calcium dehydration fixation and standard fixation for measurement of tubule diameters. Low calcium dehydration fixation data (E-F) are from Figure 1 J and K, respectively. The same relationships, but with different absolute values, are observed. Scale bars: A",B", 50 μm; C,D, 5 mm.

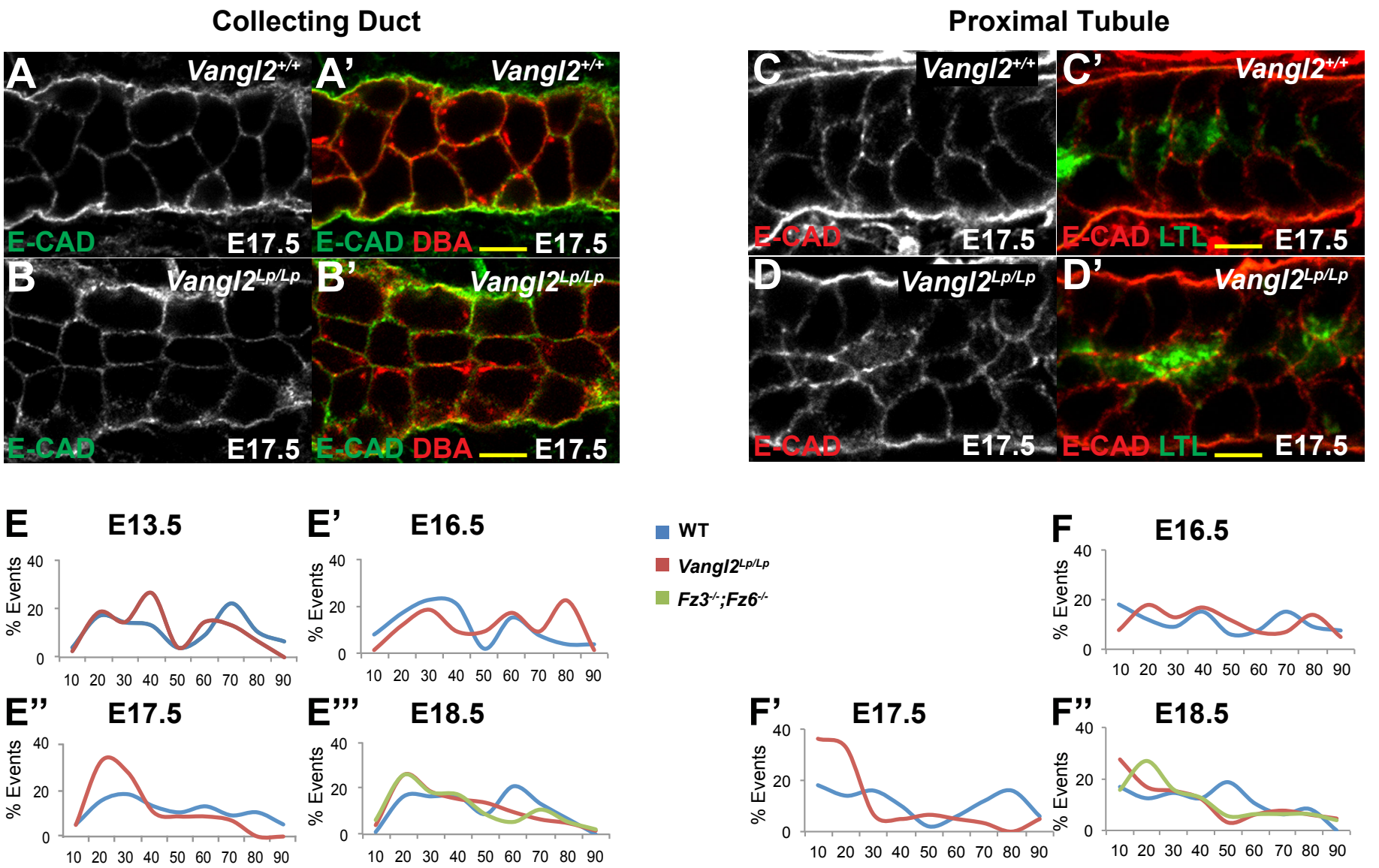
Collecting Duct
Proximal Tubule
A
Vangl2+/+
E-CAD
E17.5
A'
Vangl2+/+
E-CAD DBA
E17.5
B
Vangl2Lp/Lp
E-CAD
E17.5
B'
Vangl2Lp/Lp
E-CAD DBA
E17.5
C
Vangl2+/+
E-CAD
E17.5
C'
Vangl2+/+
E-CAD LTL
E17.5
D
Vangl2Lp/Lp
E-CAD
E17.5
D'
Vangl2Lp/Lp
E-CAD LTL
E17.5
E
E13.5
E'
E16.5
E''
E17.5
E'''
E18.5
WT
Vangl2Lp/Lp
Fz3-/-;Fz6-/-
% Events
0
20
40
10 20 30 40 50 60 70 80 90
F
E16.5
F'
E17.5
F''
E18.5
Degrees from Tubule Axis

Figure S5. Cell shapes suggesting CE in E17.5 collecting duct and proximal tubule. Related to Figure 5. (A-B') WT control or *Vangl2*$^{Lp/Lp}$ collecting ducts stained for E-CAD (green) and DBA (red) to illustrate altered cell shape and orientation in the mutant. (C-D') WT control or *Vangl2*$^{Lp/Lp}$ proximal tubules stained for E-CAD (red) and LTL (green) to illustrate altered cell shape and orientation in the mutant. (E-E''') Plots of orientation of cellular long axes relative to the tubule axis for WT control, *Vangl2*$^{Lp/Lp}$ and *Fz3*$^{-/-}$*; Fz6*$^{-/-}$ collecting ducts from E13.5 to E18.5. (F-F''') Plots of orientation of cellular long axes relative to the tubule axis for WT control, *Vangl2*$^{Lp/Lp}$ and *Fz3*$^{-/-}$*; Fz6*$^{-/-}$ proximal tubules from E16.5 to E18.5. We speculate that the biphasic distribution of wild type orientations may result from rosette configurations through which cells were shown to transition in *Xenopus* [S2]. Regardless, a shift toward the long axis is consistent with CE. Scale bars: 5 μm.

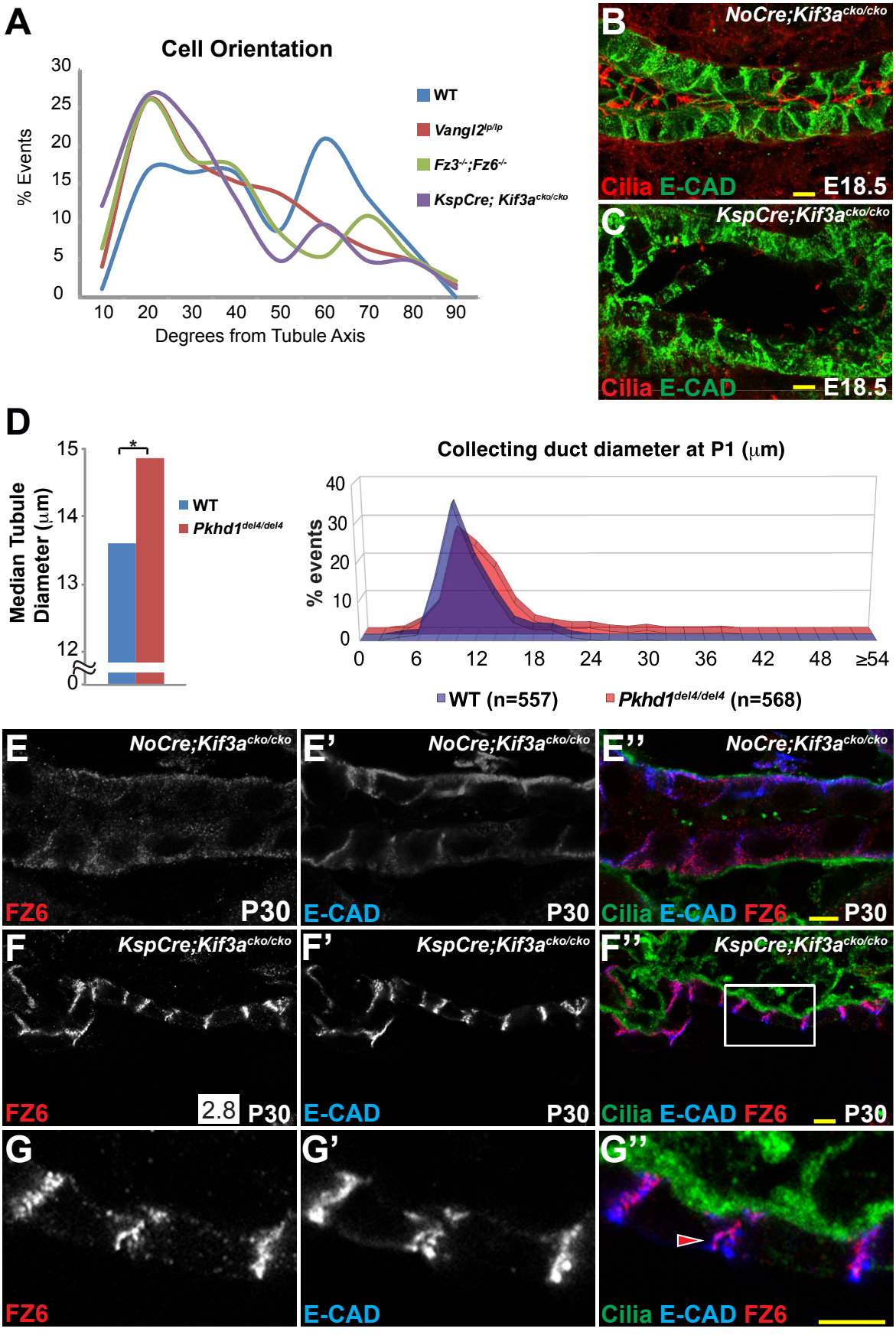
A
Cell Orientation
% Events
30
25
20
15
10
5
0
10 20 30 40 50 60 70 80 90
Degrees from Tubule Axis
WT
Vangl2lp/lp
Fz3-/-;Fz6-/-
KspCre; Kif3acko/cko
B
NoCre;Kif3acko/cko
Cilia E-CAD
E18.5
C
KspCre;Kif3acko/cko
Cilia E-CAD
E18.5
D
Median Tubule Diameter (μm)
15
14
13
12
0
*
WT
Pkhd1del4/del4
Collecting duct diameter at P1 (μm)
% events
40
30
20
10
0
0 6 12 18 24 30 36 42 48 ≥54
WT (n=557)
Pkhd1del4/del4 (n=568)
E
NoCre;Kif3acko/cko
FZ6
P30
E'
NoCre;Kif3acko/cko
E-CAD
P30
E''
NoCre;Kif3acko/cko
Cilia E-CAD FZ6
P30
F
KspCre;Kif3acko/cko
FZ6
2.8
P30
F'
KspCre;Kif3acko/cko
E-CAD
P30
F''
KspCre;Kif3acko/cko
Cilia E-CAD FZ6
P30
G
FZ6
G'
E-CAD
G''
Cilia E-CAD FZ6

Figure S6. Analysis of *Kif3a* mutant precystic and cystic kidneys. Related to Figure 6. (A) Plots of orientation of cellular long axes relative to the tubule axis for E18.5 *KspCre;Kif3a*$^{cko/cko}$ collecting ducts plotted with data for WT control, *Vangl2*$^{Lp/Lp}$ and *Fz3*$^{-/-}$*; Fz6*$^{-/-}$ collecting ducts from Figure S5E'''. (B-C) WT control (*NoCre;Kif3a*$^{cko/cko}$) and *KspCre;Kif3a*$^{cko/cko}$ collecting ducts stained at E18.5 for acetylated-α-tubulin (red; cilia) and E-Cadherin (green) showing residual short cilia in the mutant ducts. (D-D''') Median collecting duct diameter in matched littermate control and *Pkhd1*$^{del4del4-}$ mutant kidneys at P1, and distribution of diameters. . * = p<0.0001 by Mann-Whitney U test). Measurements made using the low calcium dehydration method. (E-E'') WT control (*NoCre;Kif3a*$^{cko/cko}$) and (F-F'') *KspCre;Kif3a*$^{cko/cko}$ kidneys stained at P30 for FZ6 (red), E-CAD (blue) acetylated-α-TUBULIN (green; cilia). Low levels of mostly cytoplasmic Fz6 and E-Cadherin (overexposed in E-E'') remain in the WT control collecting ducts. FZ6 and E-CAD are strongly expressed in the *KspCre;Kif3a*$^{cko/cko}$ cysts. (G-G'') Higher magnification image of a *KspCre;Kif3a*$^{cko/cko}$ mutant cyst (boxed region of F) stained for FZ6 (red) and E-CAD (blue) showing asymmetric localization of Fz6 at a cell-cell junction that separated during fixation. Scale bars: 5 μm.

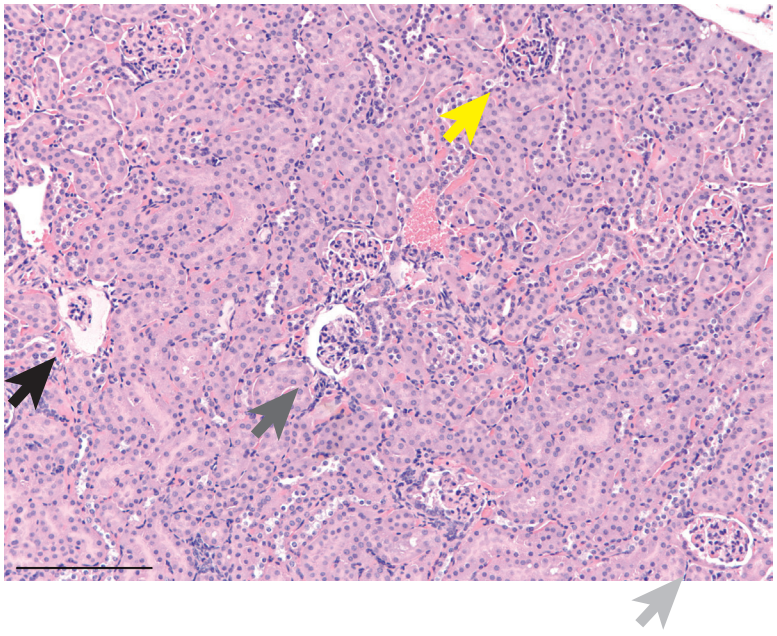

Figure S7. *Vl1,2DKO* kidney showing the GCKD phenotype. Related to Figure 7. 16w H&E stained kidney showing glomeruli with dilated capsules varying in severity (grey to black arrows) and one nearly normal glomerulus (yellow arrow). Scale bar: 200 μm.

age (weeks)	number of animals	animals with GCKD phenotype/ no. examined
3	1	0/1
16	10	1/9
24	1	
29	1	
32	1	
35	1	0/1
50	1	1/1

Table S1. Vangl1,2 DKO mice examined for cysts. Related to Figure 4.

gene name	primer, sense	primer, antisense
GAPDH	GACTTCAACAGCAACTCCCAC	TCCACCACCCTGTTGCTGTA
Pk1	GATGGAGAAAGCAAGCCAAG	TGTGCAGCATGGAAGAGTTC
Pk2	ACATGGGCACTCTCAACTCC	TGTATCCTAGGGGGTTGCTG
Pk3	TGCTGTTTCGAGTGTGAAGC	CATCACAGTATTCCGCATGG
Pk4	CCACAGGACAGTGATGAACG	CCTTCAAGCTTAGGAGGCAG
Celsr1	ATGCTGTTGGTCAGCATGTC	GGGATCTGGACAACAACCG
Celsr2	GCTGTGTGTGAGCATCTCGT	CATCATGAGTGTGCTGGTGT
Celsr3	GGAGTTGAAAGAGGCAAGGA	CTTCTCAGAGCCAGGGAGG
Fzd3	GAATCAGGTCTGGACGACTCA	CATCTGGGAGACAACATGGA
Fzd4	TGGCACATAAACCGAACAAA	TACAACGTGACCAAGATGCC
Fzd5	GGATGATTAGGGCTCCGACT	CCGCCACAGGTACCTAGCTT
Fzd6	AAAAGCTTGGCAAAGGAACA	ATTATGACCAGGGGATCGCT
Fzd8	CGGTTGTGCTGCTCATAGAA	CAGTCATCAAGCAGCAAGGA
Dvl1	GGCAACTTGGCATTGTCATC	GGTGCACGCCTACAAATTCT
Dvl2	ACACAAGCCAGGAGACAACC	TCCATGGATCAGGATTTTGG
Dvl3	CAGGGTAGCTTGGCATTGTC	GCGGCCCAGCTATAAGTTCT
Vangl1	GATGCTGTTAGGAGGTTCGG	AGTCCCGCTTCTACAGCTTG
Vangl2	TGCTGGACAAGTGGGCTTAT	GTGCGCTGCGGATACAAA
Fat1	ATTCCAAGCGACTCGAGAAA	GAGGCAAGTTTGGAGCTACG
Fat2	ACCAGCTTGGACACTTCACC	CAGCCACTTCTGTGTCCTCA
Fat3	TCACGGGAACAAACTGTGAA	CACACTCGTCCACATCATCC
Fat4	TCCGTCAGAGTGGTGTCAAG	GTTGGCCACAATGATGACAG
Dachsous1	AGTGGAACAACCACCTCTGG	GGCCTAGAGCAGTGTGGGTA
Dachsous2	TCAGCGGCAACTTACACAAC	GGTCAGACGCAAGAATCACA
Fjx1	TCTTCGGATCCAATCTCCAC	GTTCTGGAAGGGCAAACTCA
Diversin	TTGTGAGGCCCAAGGATAAG	TCCAGTCTGCTGATCACACC
Wnt1	TAGTCGCAGGTGCAGGACTC	CTCTTCGGCAAGATCGTCA
Wnt2b	TGTCTGGGTAGCGTTGACAC	CTGCTGCTGCTACTCCTGACT
Wnt3a	GGTGGCTTTGTCCAGAACAG	ACTACGTGGAGATCATGCCC
Wnt4	TCTGGATCAGGCCTTTGAGT	CCTGCGACTCCTCGTCTTC
Wnt5a	CCGGGCTTAATATTCCAATG	ACGCTTCGCTTGAATTCCT
Wnt6	CCTGCAGATGCTGGTAGGAT	CGGTAGAGCTCTCAGGATGC
Wnt7b	CTCCCCGATCACAATGATG	GCGTCCTCTACGTGAAGCTC
Wnt9b	GGAAGGGTGTCAGGACCTC	CGAGGAGATGCGAGAGTGC
Wnt11	AGGCCCTCCAGCTGTTTAC	GTCTGCGAGGCTCTGCTCT

Table S2. Primers for qPCR. Related to STAR Methods.

Supplemental References

S1. Muzumdar, M.D., Tasic, B., Miyamichi, K., Li, L., and Luo, L. (2007). A global double-fluorescent Cre reporter mouse. Genesis *45*, 593-605.

S2. Lienkamp, S.S., Liu, K., Karner, C.M., Carroll, T.J., Ronneberger, O., Wallingford, J.B., and Walz, G. (2012). Vertebrate kidney tubules elongate using a planar cell polarity-dependent, rosette-based mechanism of convergent extension. Nat Genet *44*, 1382-1387.